Article

Immunity

Brain ischemia causes systemic Notch1 activity in endothelial cells to drive atherosclerosis

Graphical abstract

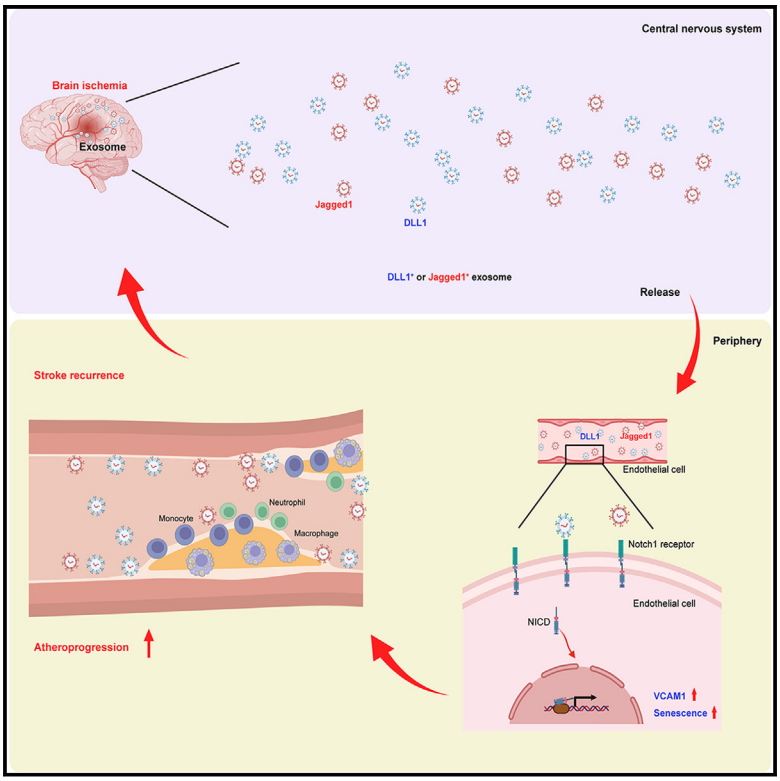

Highlights

- Stroke induces persistent endothelial cell activation and senescence in the periphery
- Circulating Notch1 ligands activate peripheral endothelial cells after brain ischemia
- Notch1 hyperactivation in endothelium augments myeloid cell adhesion
- Post-stroke atheroprogression involves Notch1-induced VCAM1 expression in endothelium

Authors

Mingming Liu, Danni Wang, Caiyun Qi, ..., Jie Zhou, Ding Ai, Qiang Liu

Correspondence

zhoujie@tmu.edu.cn (J.Z.), dingai@tmu.edu.cn (D.A.), qliu@tmu.edu.cn (Q.L.)

In brief

Whether stroke induces sustained pro-inflammatory and proatherogenic endothelial alterations in systemic vessels remains poorly understood. Liu et al. find that brain ischemia induces the persistent activation of endothelial Notch1 signaling in the periphery. A sustained increase of circulating Notch1 ligands leads to a senescent, pro-inflammatory endothelium that drives atheroprogression following stroke, which can be therapeutically targeted by blocking antibodies.

Liu et al., 2024, Immunity *57*, 2157–2172
September 10, 2024
https://doi.org/10.1016/j.immuni.2024.07.002

CellPress

Immunity

CellPress

Article

Brain ischemia causes systemic Notch1 activity in endothelial cells to drive atherosclerosis

Mingming Liu,[1] Danni Wang,[1] Caiyun Qi,[1] Ming Zou,[1] Jiawei Song,[3] Lili Li,[1] Hengchang Xie,[1] Honglei Ren,[1] Hongying Hao,[1] Guili Yang,[1] Zixiao Li,[2] Qiang Zhang,[3] Jie Zhou,[4,*] Ding Ai,[5,*] and Qiang Liu[1,6,*]

[1]Department of Neurology, Tianjin Neurological Institute, Tianjin Institute of Immunology, State Key Laboratory of Experimental Hematology, International Joint Laboratory of Ocular Diseases, Ministry of Education, Haihe Laboratory of Cell Ecosystem, Laboratory of Post-Neuroinjury Neurorepair and Regeneration in Central Nervous System Tianjin & Ministry of Education, Tianjin Medical University General Hospital, Tianjin 300052, China

[2]China National Clinical Research Center for Neurological Diseases, Beijing Tiantan Hospital, Capital Medical University, Beijing 100050, China

[3]Department of Geriatrics, Tianjin Medical University General Hospital, Tianjin Geriatrics Institute, Tianjin 300052, China

[4]Department of Immunology, Tianjin Institute of Immunology, Tianjin Medical University, Tianjin 300070, China

[5]Department of Physiology and Pathophysiology, Tianjin Medical University, Tianjin 300070, China

[6]Lead contact

*Correspondence: zhoujie@tmu.edu.cn (J.Z.), dingai@tmu.edu.cn (D.A.), qliu@tmu.edu.cn (Q.L.)

https://doi.org/10.1016/j.immuni.2024.07.002

SUMMARY

Stroke leads to persistently high risk for recurrent vascular events caused by systemic atheroprogression that is driven by endothelial cell (EC) activation. However, whether and how stroke induces sustained pro-inflammatory and proatherogenic endothelial alterations in systemic vessels remain poorly understood. We showed that brain ischemia induces persistent activation, the upregulation of adhesion molecule VCAM1, and increased senescence in peripheral ECs until 4 weeks after stroke onset. This aberrant EC activity resulted from sustained Notch1 signaling, which was triggered by increased circulating Notch1 ligands DLL1 and Jagged1 after stroke in mice and humans. Consequently, this led to increased myeloid cell adhesion and atheroprogression by generating a senescent, pro-inflammatory endothelium. Notch1- or VCAM1-blocking antibodies and the genetic ablation of endothelial Notch1 reduced atheroprogression after stroke. Our findings revealed a systemic machinery that induces the persistent activation of peripheral ECs after stroke, which paves the way for therapeutic interventions or the prevention of recurrent vascular events following stroke.

INTRODUCTION

Stroke causes a markedly increased risk for recurrent atherothrombotic events in systemic vascular territories. In stroke survivors, the risk of suffering a recurrence is up to 30% by 5 years, which is about 9 times the risk of stroke in the general population.[1,2] The risk is particularly high early after the first stroke, i.e., up to 15% by 1 year, which is about 15 times the risk in the general population.[1–4] These findings indicate that stroke leads to systemic adverse vascular responses, which remains elevated even years after the first stroke. Stroke activates the immune system, leading to systemic vascular inflammation. Recent evidence demonstrates that brain ischemia mobilizes pro-inflammatory monocytes and accelerates their entry into peripheral arterial plaques after the initial stroke onset.[5] Although stroke-induced monocyte activation and their entry into peripheral arterial plaques have been depicted, little is known about the endothelial-specific alterations in response to stroke and their potential impact on atherosclerotic progression.

As a driver of atherosclerosis, endothelial cells (ECs) govern the site specificity of atherogenesis and express adhesion molecules to instruct myeloid cell entry into lesion sites.[6] The existence of persistent vascular inflammation and exacerbated systemic athroprogression after stroke suggests the postulation that acute ischemic brain injury may prime the entire vasculature to facilitate monocyte entry into the plaque and exacerbate plaque expansion, leading to higher risk for stroke recurrence and increased susceptibility to further cerebrovascular or cardiovascular events. In this regard, a number of key questions remain to be addressed. First, the dynamics of endothelial-specific alterations is unclear after stroke, which is essential to understand whether ECs may exert long-term impact on vascular inflammation and atherosclerotic progression. Second, the particular signals that drive endothelial-specific alterations after stroke are to be identified and how are these signals conveyed to the peripheral ECs to produce a systemic vascular response? Third, the endothelial mechanisms that control monocyte recruitment into plaque lesions in the periphery remain relatively unexplored. Finally, it remains uncertain whether increased remote plaque inflammation following stroke can be suppressed by targeting endothelial-specific alterations.

In this study, we found that brain ischemia induces persistent activation of endothelial Notch1 signaling in the periphery. A

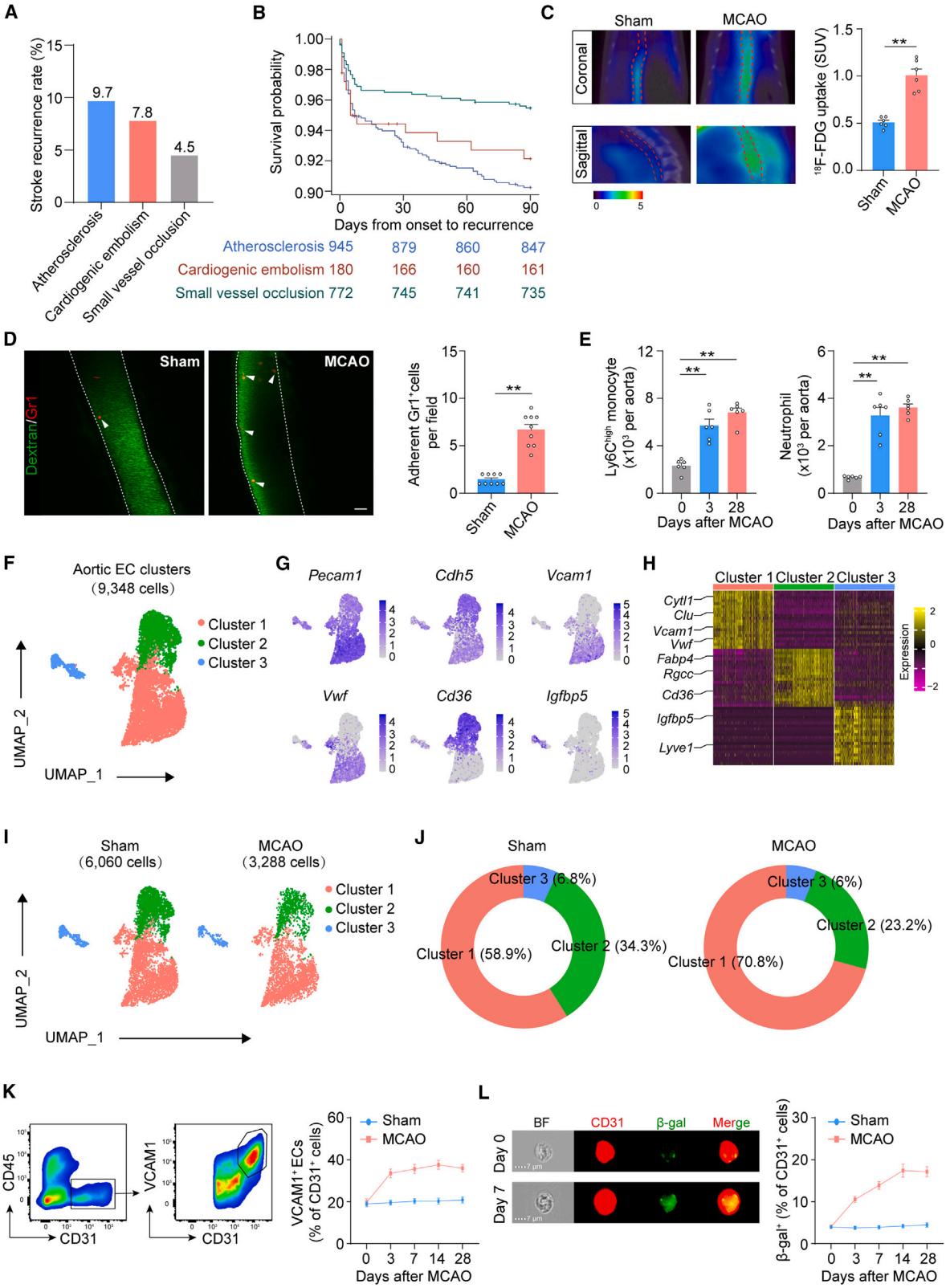

(legend on next page)

sustained increase in circulating Notch1 ligands leads to a senescent, pro-inflammatory endothelium that drives atheroprogression following stroke, which can be therapeutically targeted by blocking antibodies.

RESULTS

Brain ischemia induces sustained activation and senescence of ECs in the periphery

To assess the recurrence rate of cerebrovascular events in stroke survivors, we used pooled data from individuals enrolled in the Third China National Stroke Registry (CNSR-III) (n = 10,348) to measure stroke recurrence rate, related causes, and mortality during first 3 months after initial onset.[7] Stroke recurrence rates resulted from atherosclerosis in large artery, cardiogenic embolism, and small vessel occlusion were 9.7%, 7.8%, and 4.5% at the first 3 months after stroke onset, respectively (Figure 1A). The stroke recurrence and mortality during the first 3 months after stroke onset were mainly caused by atherosclerosis in large artery versus cariogenic embolism or small vessel occlusion (Figures 1A and 1B), suggesting the limitations of current strategies for secondary stroke prevention to effectively reduce early stroke recurrent events related to atherosclerosis in large artery.

To gain insights into the aorta characteristics displayed at steady state and stroke, using micro-positron-emission tomography (PET) and computed tomography (CT) scanning, we measured the uptake of ^{18}F-fluorodeoxyglucose (FDG), a glucose uptake tracer, in aorta of mice subjected to experimental stroke induced by transient middle cerebral artery occlusion (MCAO). At day 3 after MCAO and reperfusion, we found an increase in ^{18}F-FDG uptake in the aorta (Figure 1C), suggesting that stroke induces increased activity of cells in large artery such as aorta after stroke. Using intravital fluorescence microscopy, we found markedly increased adhesion of Gr1$^+$ myeloid cells (i.e., neutrophils and monocytes) on mesenteric vessels in MCAO mice versus sham controls (Figure 1D). Additionally, neutrophils and Ly6C^{high} monocytes adhesion to the aorta were augmented at day 3 after MCAO and persisted at least until day 28 after onset (Figures 1E and S1A), suggesting that stroke imposes a long-term impact on large arteries.

As ECs are central to controlling immune cell trafficking, vascular inflammation, and atherosclerosis, we sought to understand how ECs in large arteries sense and adapt to brain ischemia. For this purpose, single-cell suspensions were prepared from sorted CD31$^+$ ECs isolated from aorta tissues in groups of sham mice or MCAO mice at day 3 after onset for single-cell RNA sequencing (scRNA-seq). After Louvain clustering of 22,055 cells by graph-based clustering and uniform manifold approximation and projection (UMAP) (Figure S1B), clusters were annotated on the basis of gene signatures from ECs (*Pecam1*, *Cdh5*, and *Erg*), smooth muscle cells (*Tagln* and *Acta2*), fibroblasts (*Dcn*, *Lum*, and *Pdgfra*), lymphoid cells (*Cd3d* and *Cd8a*), myeloid cells (*S100a9*, *S100a8*, and *Cd14*), and pericytes (*Rgs5* and *Vtn*) (Figures S1C and S1D). Among 9,348 ECs, we identified 3 EC clusters (Figure 1F). All three EC clusters expressed *Pecam1* and *Cdh5* (Figure 1G). Cluster 1 highly expressed *Vcam1*, *Vwf*, and other genes such as *Cytl1* and *Clu* (Figures 1G and 1H). Cluster 2 expressed genes involved in lipid transport, including *Cd36*, *Fabp4*, and *Rgcc* (Figures 1G and 1H). Cluster 3 expressed markers of lymphatic identity, including *Igfbp5* and *Lyve1* (Figures 1G and 1H). Cluster 1 and cluster 2 were distinctive and possessed 944 and 628 differentially expressed genes (DEGs), respectively. Cluster 3 was an intermediate population with the majority of DEGs overlapping with cluster 1 or cluster 3 (Figure S1E). A marked increase in cluster 1 was observed in MCAO mice versus sham mice (Figures 1I and 1J).

Flow cytometry analysis revealed an increase in vascular cell adhesion molecule 1 (VCAM1)-expressing ECs in MCAO mice versus sham mice at least until day 28 after MCAO and reperfusion (Figure 1K), along with an increase of senescence markers,

Figure 1. Brain ischemia induces sustained activation and senescence of ECs in the periphery

(A and B) The Third China National Stroke Registry (CNSR-III) is a nationwide, prospective, and multicenter clinical registry study that recruited patients with acute ischemic cerebrovascular events in China between August 2015 and March 2018. Stroke recurrence and mortality of patients in CNSR-III within 3 months after the onset of ischemic stroke.

(A) The rates of stroke recurrence resulted from large artery atherosclerosis, cardiogenic embolism, and small vessel occlusion during first 3 months after stroke onset in CNSR-III.

(B) Survival probability of patients with indicated diseases.

(C) ^{18}F-FDG PET-CT images of aorta at day 3 after MCAO; dashed red lines show the regions of interest for quantification. Bar graphs showing the measurement of standard uptake value (SUV). n = 6 mice per group. Data were representative of three independent experiments.

(D) Intravital microscopic photographs and quantitation of Gr1$^+$ cells (monocytes and neutrophils, red) that adhered to mesenteric vessels (green) at day 3 after MCAO. Scale bars, 100 μm. n = 9 mice per group. Data were representative of three independent experiments.

(E) Flow cytometry assessment of neutrophils and Ly6C^{high} monocytes adhesion to the aorta at indicated time points after MCAO. n = 6 mice per group. Data were representative of three independent experiments.

(F–J) Sorted endothelial cells (CD31$^+$) from wild-type mice following sham surgery (steady state) and day 3 after MCAO were processed individually for scRNA-seq (10× Genomics).

(F) UMAP plots of the combined analysis of sham and day 3 after MCAO visualized together.

(G) Feature plots illustrating expression of subset-defining genes.

(H) Heatmap of the top 10 differentially expressed genes in each cluster (logFC threshold = 0.2, min.pct = 0.2, adjusted p value < 0.05).

(I) UMAP plots of sham and day 3 after MCAO visualized separately.

(J) Quantification of the relative percentage of each cluster under each condition.

(K) Flow cytometry gating strategy of CD45$^-$CD31$^+$VCAM1$^+$ ECs (left) and frequency of CD45$^-$CD31$^+$VCAM1$^+$ cells (right) in the aorta at indicated time points after MCAO. n = 11 mice per group. Data were representative of four independent experiments.

(L) Imaging cytometry analysis of β-gal$^+$ ECs at indicated time points after MCAO. β-gal in ECs after MCAO (left), quantitation of the relative percentage of β-gal$^+$ in the aorta (right) at indicated time points after MCAO. n = 11 mice per group. Data were representative of four independent experiments. Mean ± SEM. $^{**}p < 0.01$. Two-tailed unpaired Student's t test (C and D), one-way ANOVA followed by Tukey post hoc test (E).

See also Figure S1.

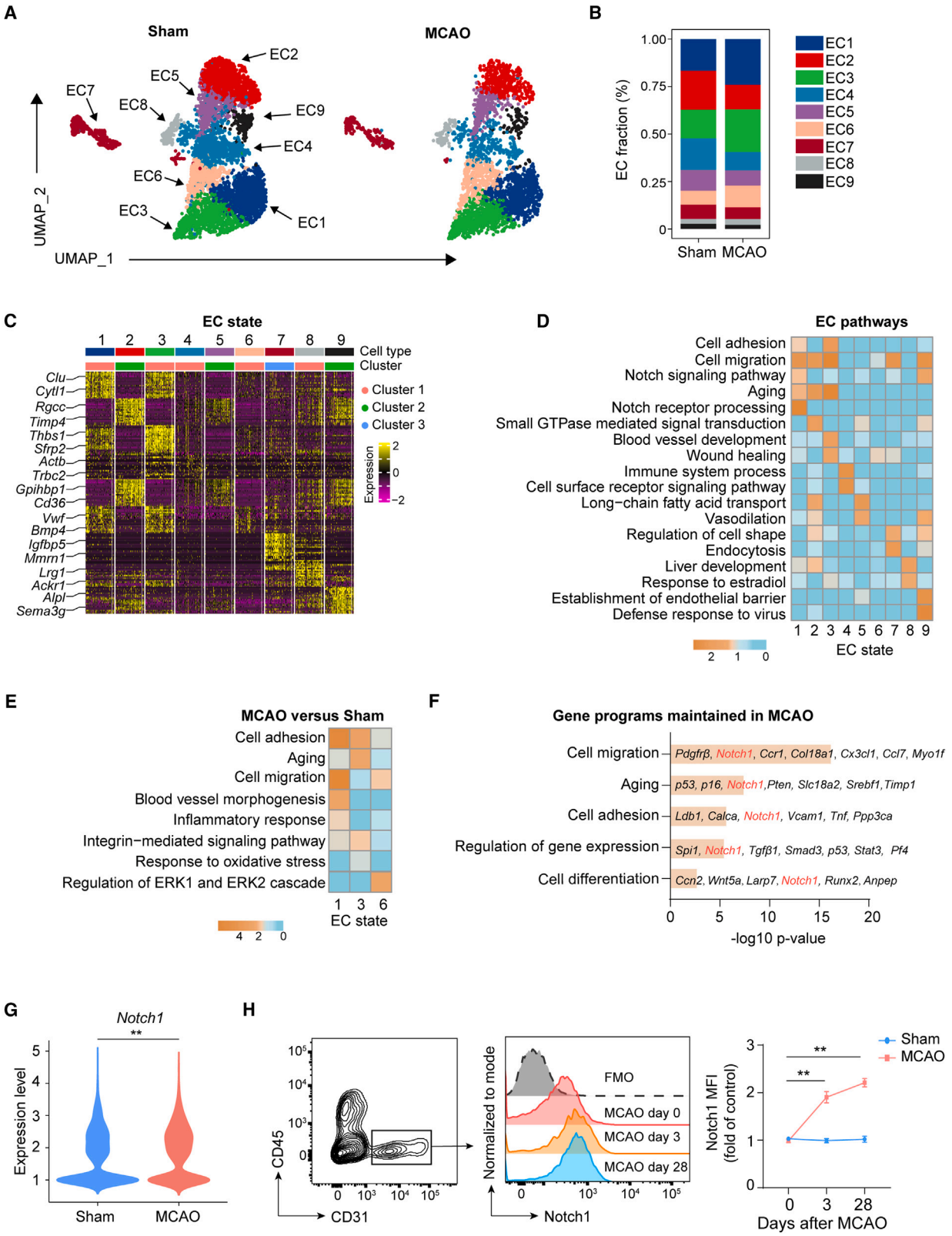

Figure 2. Brain ischemia induces sustained EC Notch1 activation in the periphery

(A) High-resolution clustering identifies nine endothelial cell states (EC1–EC9) in sham and day 3 after MCAO, UMAP plots split by conditions.

(B) Abundance of each cell state (EC1–EC9) across conditions.

(legend continued on next page)

including P16, P53, and senescence-associated β-galactosidase (β-gal) (Figures 1L and S1F–S1H), suggesting that stroke induces the persistent activation of remote ECs in the periphery and senescence in these cells. Together, these results demonstrate profound and sustained changes in peripheral ECs in response to brain ischemia.

Brain ischemia leads to sustained EC Notch1 activation in the periphery

To characterize the heterogeneity and phenotype of peripheral ECs in response to brain ischemia, we performed single-cell analysis of three EC clusters. EC clusters were classified into 9 distinct states. We found that the proportions of EC1, EC3, and EC6 were higher in MCAO mice versus sham controls (Figures 2A–2C). Cluster 1 of ECs consisted of 5 cell states (EC1, 3, 4, 6, and 8) (Figure 2C); EC1 expressing *Cytl1* or *Clu* was enriched in several pathways related to cell adhesion, cell migration, Notch signaling pathway, aging, and Notch receptor processing (Figure 2D). EC3 expressing *Thbs1* and *Sfrp2* had enriched expression of pathways mediating cell adhesion, cell migration, aging, blood vessel development, and wound healing (Figure 2D). EC6 expressing *Vwf* and *Bmp4* had enriched expression of pathways in cell migration and wound healing (Figure 2D). The augmented enrichment of pathways in EC1, EC3, and EC6 in brain ischemia suggests that these cell states were responsive to stroke onset. These stroke-induced genes were mapped to pathways involved in blood vessel morphogenesis (EC1), response to oxidative stress (EC3), and positive regulation of ERK1 and ERK2 cascade (EC6) (Figure 2E). We also observed several pathways shared among EC1, EC3, and EC6 such as cell adhesion, aging, and cell migration (Figure 2E). Then, we observed that ECs, irrespective of clusters or cell states, were enriched in pathways related to cell migration, aging, and cell adhesion after brain ischemia. Of note, these pathways consistently involve *Notch1*, which was constitutively upregulated in ECs after brain ischemia (Figures 2F, 2G, and S2A). In contrast, the expression of *Notch2*, *Notch3*, and *Notch4* remained unaltered (Figure S1I).

Similarly, flow cytometry analysis also revealed the upregulation of Notch1 receptor in ECs from the aorta of MCAO mice versus sham controls (Figure 2H). The expression of NICD1, an activated form of Notch1, was increased in ECs from the aorta of MCAO mice versus sham controls (Figure S1J). As NICD is known to interact with transcription factors such as CBF1 and induce the transcription of downstream genes.[8,9] We have screened the alterations of related genes and found an increase of *Nfκb* in ECs of MCAO mice (Figure S1K). These results have demonstrated that brain ischemia induces sustained EC Notch1 activation in the periphery, suggesting that the activation and senescence of vascular ECs during stroke may involve Notch1 signaling.

A sustained increase in circulating Notch1 ligands is evident following brain ischemia

As an essential mediator of cell-cell communication, Notch signaling in remote target cells can be activated by secreted Notch ligands via exosomes from cellular sources without physical contact.[10,11] To investigate how stroke induces remote EC Notch1 activation in the periphery, we collected circulating exosomes from groups of MCAO or sham mice to measure their morphology and size using transmission electron microscopy (TEM) and nanoparticle tracking analysis (NTA) (Figure 3A). To assess the expression of Notch ligands on circulating exosomes, we measured the expression of DLL1, DLL3, DLL4, Jagged1, and Jagged2 by ELISA. We found an increase in DLL1 and Jagged1 in circulating exosomes until day 28 after MCAO versus sham controls (Figures 3B and S2A). In contrast, the concentrations of DLL3, DLL4, and Jagged2 were not substantially altered (Figures S2B–S2D). In patients with ischemic stroke and healthy controls, we quantified the factors in circulating exosomes. Among 80 factors measured by a proteome profiler, we found that DLL1 and Jagged1 are highly expressed in circulating exosomes from patients with ischemic stroke (day < 2 after onset) (Figure 3C). Similarly, ELISA analysis revealed an increase in DLL1 and Jagged1 in circulating exosomes from patients with ischemic stroke at early stage (day < 2 after onset) or late stage (day 14 after onset) versus controls (Figure 3D).

To determine the cellular sources of circulating exosomes expressing Notch1 ligands after brain ischemia, we used imaging cytometry analysis to measure circulating exosomes. We found an increase in $DLL1^+P2RY12^+CX3CR1^+$ or $Jagged1^+P2RY12^+CX3CR1^+$ circulating exosomes in patients with ischemic stroke versus controls, suggesting that exosomes derived from $P2RY12^+CX3CR1^+$ cells (myeloid cells) mainly contribute to the increase in circulating Notch1 ligands after stroke (Figure 3E). In contrast, no significant alterations were noted in $DLL1^+$ or $Jagged1^+$ exosomes derived from $L1CAM^+$ cells (neurons) or $GFAP^+$ cells (astrocytes) (Figure 3E). Additionally, an increase in circulating $DLL1^+$ or $Jagged1^+$ exosomes derived from $P2RY12^+CX3CR1^+$ cells was also found in MCAO mice on day 3 and day 28 after surgery (Figure S2E). Flow cytometry analysis also revealed an increase in $DLL1^+$ and $Jagged1^+$ $P2RY12^+CX3CR1^+$ cells in MCAO mice until day 28 after surgery (Figures 3F and 3G). Additionally, the expression of DLL1 and Jagged1 was not substantially altered in $GFAP^+$ cells and $L1CAM^+$ cells (Figure S2F).

(C) Heatmap of the top 10 differentially expressed genes in each cell state (logFC threshold = 0.2, min.pct = 0.2, adjusted p value < 0.05). The color bar denotes the high-resolution state (top; EC1–EC9), low-resolution cluster (clusters 1–3; center).
(D) Pathway enrichment analysis (gProfiler, Gene Ontology [GO] biological processes) using differentially expressed genes (DEGs) for each cell state (EC1–EC9). Heatmap shows the $-\log_{10} p$ value of indicated factors.
(E) Pathway enrichment analysis (gProfiler, GO biological processes, Kyoto Encyclopedia of Genes and Genomes [KEGG]) using DEGs upregulated at day 3 after MCAO relative to sham for selected cell states. Heatmap shows the $-\log_{10} p$ value of indicated factors.
(F) DEGs of endothelial cells relative to sham and day 3 after MCAO, the overlap of these DEGs were used for pathway enrichment analysis (gProfiler, GO biological processes).
(G) Violin graph shows *Notch1* expression in endothelial cells.
(H) Flow cytometry analysis of Notch1 expression in endothelial cells of aorta at indicated time points after MCAO. $n = 6$ per group. Data were representative of three independent experiments. Mean ± SEM. $^{**}p < 0.01$. Two-way ANOVA followed by Tukey post hoc test (H).
See also Figure S1.

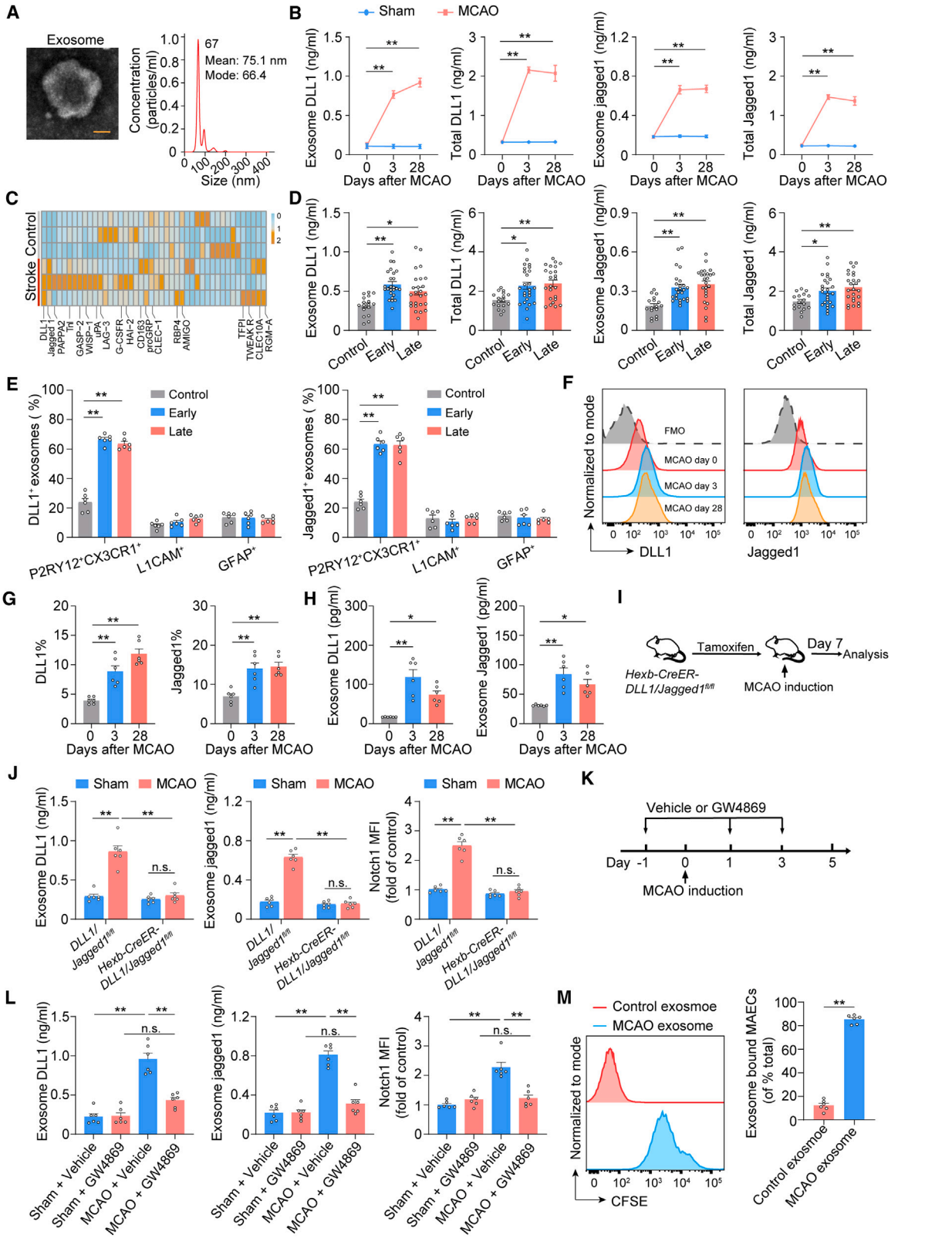

(legend on next page)

To directly measure DLL1$^+$ or Jagged1$^+$ exosomes derived from P2RY12$^+$CX3CR1$^+$ cells, we isolated P2RY12$^+$CX3CR1$^+$ cells from the brains of MCAO mice and sham controls. After 24 h culture, we found an increase in DLL1$^+$ or Jagged1$^+$ exosomes in collected culture medium from P2RY12$^+$CX3CR1$^+$ cells in MCAO mice versus controls (Figure 3H). To test whether P2RY12$^+$CX3CR1$^+$ cells are a major source of circulating DLL1$^+$ or Jagged1$^+$ exosomes, we used *Hexb-CreERT2-DLL1/Jagged1*$^{fl/fl}$ mice that are devoid of DLL1 and Jagged1 in microglia. We found that genetic deficiency of DLL1 and Jagged1 in microglia diminished the increase in circulating DLL1$^+$ or Jagged1$^+$ exosomes and the activation of Notch1 in peripheral ECs from MCAO mice (Figures 3I and 3J). Notably, the expressions of VCAM1, P16, and P53 in ECs were reduced in MCAO *Hexb-CreERT2-DLL1/Jagged1*$^{fl/fl}$ mice that are devoid of DLL1 and Jagged1 in microglia (Figure S2G). Flow cytometry analysis revealed that Ly6C^{high} monocytes and neutrophils in aortic tissues were decreased in MCAO *Hexb-CreERT2-DLL1/Jagged1*$^{fl/fl}$ mice (Figure S2H). Brain infarct volume was similar in *Hexb-CreERT2-DLL1/Jagged1*$^{fl/fl}$ MCAO mice versus *DLL1/Jagged1*$^{fl/fl}$ MCAO mice (Figure S2I).

To examine the impact of exosome release from the ischemic brain on ECs in the periphery, we perform intracerebroventricular injection of GW4869, an inhibitor of exosome release (Figure 3K). After GW4869 administration, we found a reduction in DLL1 and Jagged1 in circulating exosomes in MCAO mice (Figure 3L), together with reduced activation and senescence of ECs in the periphery (Figure S2J). Notably, Ly6C^{high} monocytes and neutrophils in aortic tissues were reduced in MCAO mice after GW4869 administration (Figure S2K). In addition, GW4869 administration did not substantially alter brain infarct volume in MCAO mice (Figure S2L).

To assess the direct impact of P2RY12$^+$CX3CR1$^+$ cells-derived exosomes on peripheral ECs, we co-cultured mouse aortic ECs (MAECs) with exosomes from P2RY12$^+$CX3CR1$^+$ cells in MCAO mice or sham controls. We found that P2RY12$^+$CX3CR1$^+$ cells-derived exosomes can bind to MAECs, leading to the upregulation of Notch1, VCAM1, and senescence markers P16 and P53 (Figures 3M and S3A). Additionally, the expression of DLL1 or Jagged1 in the peripheral monocytes and neutrophils remains low after brain ischemia, suggesting its minimal contribution to circulating DLL1$^+$ or Jagged1$^+$ exosomes and EC activation (Figures S3B and S3C). Using an inhibitor of nuclear factor κB (NF-κB), we found that Notch1 activation-induced upregulation of VCAM1 is diminished (Figure S3D), suggesting that NF-κB is involved in VCAM1 upregulation in ECs. These results suggest that P2RY12$^+$CX3CR1$^+$ cells-derived DLL1$^+$ or Jagged1$^+$ exosomes can be released into the periphery and contribute to EC Notch1 activation after stroke.

As high-mobility group box 1 (HMGB1) is a prominent brain-released alarmin.[5] To assess circulating HMGB1 after stroke, we measured circulating HMGB1 by ELISA. We found an increase in circulating HMGB1 until day 28 after MCAO versus sham controls (Figure S3E). In addition, we performed an analysis of single-cell RNA sequencing to assess the expression of *Ager* (receptor of HMGB1). The data showed that *Ager* expression was minimal and not substantially altered in MCAO mice versus sham controls (Figure S3F). We also measured Notch1 activation in MCAO mice receiving an anti-HMGB1 neutralizing antibody. We found that neutralization of HMGB1 did not

Figure 3. A sustained increase of circulating Notch1 ligands is evident following brain ischemia

(A) TEM image of purified exosomes from plasma, characterization of purified exosomes using NTA. Scale bars, 50 nm.

(B) ELISA of circulating exosomal DLL1, total DLL, exosomal Jagged1, and total Jagged1 in plasma at indicated time points after MCAO. $n = 6$ per group. Data were representative of three independent experiments.

(C) Heatmap showing proteins in circulating exosomes sorted from patients with stroke and healthy control individuals. Heatmap shows the Z scores of indicated factors. $n = 3$ per group.

(D) ELISA of circulating exosomal DLL1, total DLL1, exosomal Jagged1, and total Jagged1 in plasma sorted from patients with stroke and healthy control individuals. $n = 17, 25, 25$ in group of healthy control, stroke patients at early time point (day < 2 after onset) and late time point (day 14 after onset). Data were representative of four independent experiments.

(E) Quantification of circulating DLL1$^+$ or Jagged1$^+$ exosomes from P2RY12$^+$CX3CR1$^+$ cells (myeloid cells), L1CAM$^+$ cells (neurons), and GFAP$^+$ cells (astrocytes) in plasma from patients with stroke and healthy controls. Early time point: day < 2 after onset, late time point: day 14 after onset. $n = 6$ per group. Data were representative of three independent experiments.

(F) Flow cytometry analysis of DLL1 and Jagged1 expression in P2RY12$^+$CX3CR1$^+$ cells at indicated time points after MCAO.

(G) Quantification of DLL1 and Jagged1 expression in P2RY12$^+$CX3CR1$^+$ cells at indicated time points after MCAO. $n = 6$ per group. Data were representative of three independent experiments.

(H) P2RY12$^+$CX3CR1$^+$ cells from sham or MCAO mice were isolated and cultured in medium for 24 h, and then, the culture medium was collected to purified exosomes (left), ELISA of exosomal DLL1 (middle) and exosomal Jagged1(right) in culture medium of P2RY12$^+$CX3CR1$^+$ cells at indicated time points after MCAO. $n = 6$ per group. Data were representative of three independent experiments.

(I) *Hexb-CreER-DLL1/Jagged1*$^{fl/fl}$ mice received daily tamoxifen treatment for 5 consecutive days prior to MCAO induction and were sacrificed 7 days after surgery.

(J) ELISA measurement of exosomal DLL1 (left) and exosomal Jagged1 (middle) in plasma at indicated condition after MCAO. Flow cytometry assessment of Notch1 (right) in ECs of aorta at indicated time points after MCAO. $n = 6$ per group. Data were representative of three independent experiments.

(K) Flow chart illustrates drug administration and experimental design. Mice received intracerebroventricular injection of GW4869 or vehicle at 1 day prior to MCAO and every 2 days thereafter until the end of experiment.

(L) ELISA measurement of exosomal DLL1 (left) and exosomal Jagged1 (middle) in plasma at indicated condition after MCAO. Flow cytometry assessment of Notch1 (right) in ECs of aorta at indicated time points after MCAO. $n = 6$ per group. Data were representative of three independent experiments.

(M) Exosomes from P2RY12$^+$CX3CR1$^+$ cells in MCAO mice or sham controls were labeled with CFSE. Flow cytometry assessment of MAECs after incubation with CFSE-labeled P2RY12$^+$CX3CR1$^+$ cells-derived exosomes for 2 h (left). The proportion of exosome-bound cells is shown (right). $n = 6$ per group. Data were representative of three independent experiments. Mean ± SEM. $^*p < 0.05$, $^{**}p < 0.01$. n.s., not significant. One-way ANOVA followed by Tukey post hoc test (D, E, G, and H), two-way ANOVA followed by Tukey post hoc test (B and J–L), Two-tailed unpaired Student's t test (M).

See also Figures S2 and S3.

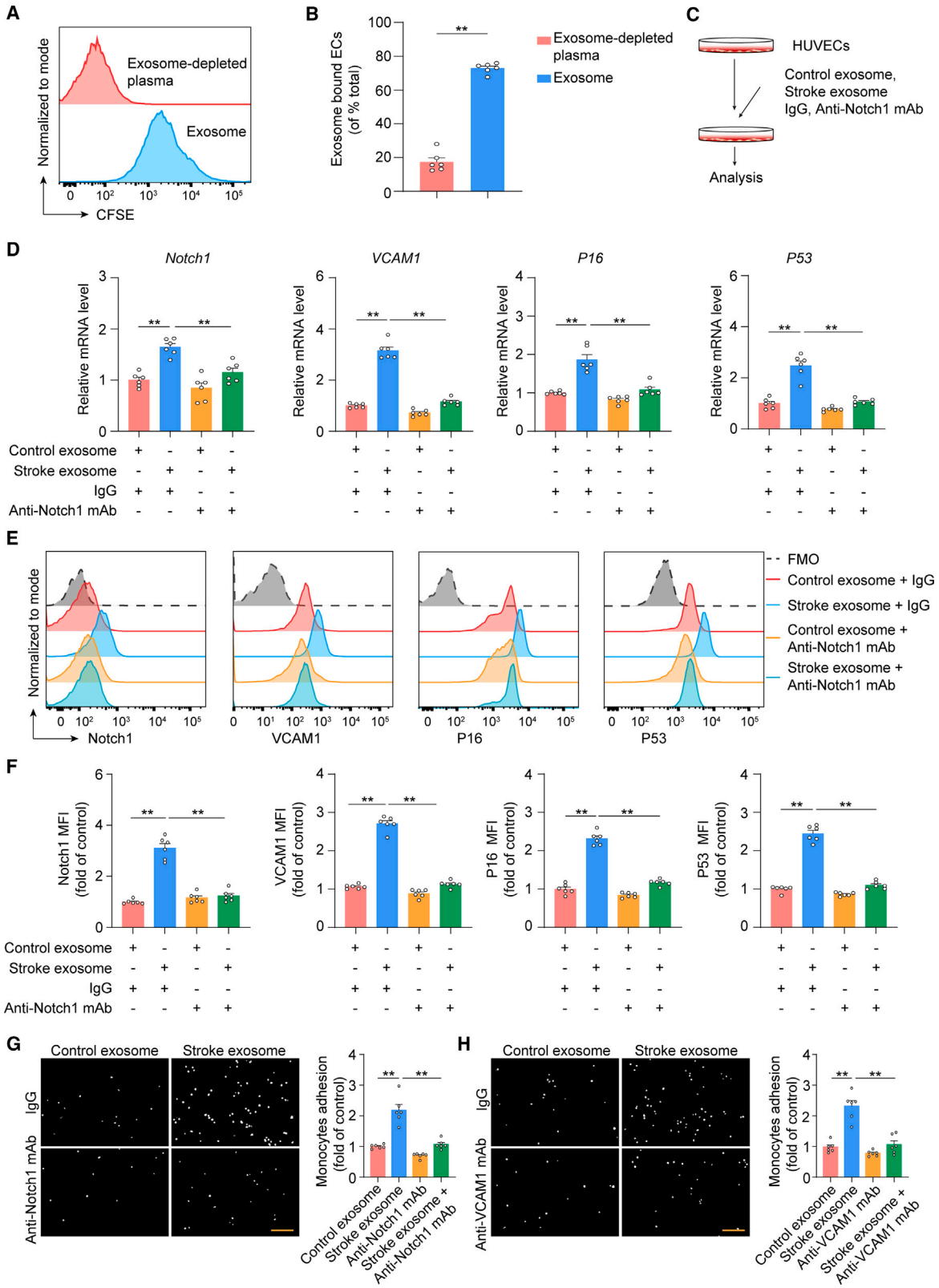

Figure 4. Circulating exosomes from patients with ischemic stroke induce endothelial Notch1 activation and cellular senescence

(A) Flow cytometry histogram of HUVECs after incubation with CFSE-labeled-plasma derived exosomes for 2 h.

(B) The proportion of exosome-bound cells is shown. *n* = 6 per group. Data were representative of three independent experiments.

(legend continued on next page)

substantially alter the activation of Notch1 signaling and the expressions of VCAM1, P16, and P53 in ECs following MCAO (Figure S3G). These results imply that stroke-induced activation of ECs may differ from the effects induced by post-ischemic release of alarmins such as HMGB1 as previously described.[5]

Circulating exosomes from patients with ischemic stroke induce endothelial Notch1 activation and cellular senescence

To test whether circulating exosomes are sufficient to induce endothelial Notch1 activation and cellular senescence, we co-cultured human umbilical vein ECs (HUVECs) with circulating exosomes from patients with ischemic stroke or controls. We found that circulating exosomes from patients with ischemic stroke bind to HUVECs (Figures 4A and 4B), leading to the upregulation of *Notch1*, adhesion molecule *VCAM1,* and senescence markers *P16* and *P53* mRNA (Figures 4C and 4D).

Next, we tested whether circulating exosome-induced EC activation and senescence depend on Notch1 signaling. For this purpose, anti-Notch1 monoclonal antibody (mAb) was used to block Notch1 signaling. We found that circulating exosome-induced increase of *Notch1*, *VCAM1*, *P16*, and *P53* mRNA was abolished in HUVECs receiving anti-Notch1 mAb treatment versus immunoglobulin G (IgG) control (Figures 4C and 4D). Notably, anti-Notch1 mAb treatment ablated the increase of Notch1, VCAM1, P16, and P53 in HUVECs treated with circulating exosomes from patients with ischemic stroke (Figures 4E and 4F).

To test the effects of circulating exosome-induced VCAM1 upregulation on leukocyte adhesion, we co-cultured THP-1 (a human monocytic leukemia cell line) cells with HUVECs treated with circulating exosomes from patients with ischemic stroke or controls. We found increased adhesion of THP-1 cells to HUVECs treated with circulating exosomes from patients with ischemic stroke, which was abolished by treatment with anti-Notch1 mAb or anti-VCAM1 mAb (Figures 4G and 4H). Together, these results suggest that circulating exosomes from patients with ischemic stroke are sufficient to induce EC Notch1 activation and senescence.

VCAM1 blockade suppresses stroke-induced atheroprogression

To test the contributions of VCAM1 to stroke-induced vascular inflammation, we treated wild-type mice with anti-VCAM1 mAb or IgG control for 2 weeks starting from day 3 after MCAO and reperfusion (Figure 5A). Flow cytometry analysis revealed that anti-VCAM1 mAb diminished brain ischemia-induced increase of Ly6C^{high} monocytes and neutrophils in aortic tissues (Figure 5B).

To test the contributions of VCAM1 to stroke-induced growth of atherosclerotic lesions, we measured the effects of VCAM1 blockade on stroke-induced plaque growth and vascular inflammation using atherosclerosis-prone apolipoprotein E-deficient (*apoE*$^{-/-}$) mice. We found that MCAO induced an increase of atherosclerotic lesions and accumulation of infiltrating accumulation of monocytes within lesion sites in *apoE*$^{-/-}$ mice, which was diminished by VCAM1 blockade using anti-VCAM1 mAb (Figures 5C–5F and S4A), along with increased collagen content and similar α smooth muscle actin (αSMA)-positive area (Figures 5G, S4B, and S4C). VCAM1 blockade did not alter circulating triglyceride (TG), cholesterol (CHO), low-density lipoprotein cholesterol (LDL-C), and high-density lipoprotein cholesterol (HDL-C) in *apoE*$^{-/-}$ mice subjected to MCAO or sham surgery (Figure 5H). Delayed treatment with anti-VCAM1 mAb did not substantially alter brain lesion volume in MCAO mice (Figures S4D and S4E). Additionally, we found that high-fat diet treatment alone did not substantially alter the expressions of Notch1, VCAM1, P16, and P53 in ECs from MCAO mice or sham controls (Figure S4F). Together, these results suggest the necessity of VCAM1 in stroke-induced atheroprogression.

Disruption of endothelial Notch1 attenuates stroke-induced atheroprogression

To investigate the effects of EC Notch1 on vascular inflammation in the periphery, we generated *Tie2Cre-Notch1*$^{fl/-}$ and *Notch1*$^{fl/-}$ mice. We found that the expressions of VCAM1, P16, and P53 in ECs were reduced in MCAO *Tie2Cre-Notch1*$^{fl/-}$ mice (Figures S5A and S5B), along with the reduction of infiltrating Ly6C^{high} monocytes and neutrophils in aortic tissues (Figure S5C). To assess the effects of disrupting endothelial Notch1 signaling on stroke-induced growth of atherosclerotic lesions and vascular inflammation, we generated *Tie2Cre-Notch1*$^{fl/-}$*apoE*$^{-/-}$ and *Notch1*$^{fl/-}$*apoE*$^{-/-}$ mice. These mice received a high-fat diet for 8 weeks starting from 4 weeks prior to MCAO surgery (Figure 6A). We found the atherosclerotic lesions were reduced in whole aorta and aortic roots in *Tie2Cre-Notch1*$^{fl/-}$*apoE*$^{-/-}$ versus *Notch1*$^{fl/-}$*apoE*$^{-/-}$ mice after stroke, along with a decrease in infiltrating monocytes and oil red O-positive area, and similar collagen content in atherosclerotic plaque (Figures 6B–6E, S5D, and S5E), whereas no significant difference was noted in *Tie2Cre-Notch1*$^{fl/-}$*apoE*$^{-/-}$ mice in sham group versus MCAO group (Figures 6B–6E). A similar αSMA-positive area was also observed (Figure S5F). Circulating TG, total CHO, LDL-C, and HDL-C were similar among the groups of mice (Figure 6F). The brain infarct size and the release of DLL1^{+} or Jagged1^{+} exosomes after stroke

(C–F) HUVECs were pretreated with IgG or anti-Notch1 antibodies at 10 μg/mL for 2 h, then given control exosomes or stroke exosomes (15 μg/mL) for 24 h.
(D) mRNA expression of *Notch1*, *VCAM1*, *P16*, and *P53* were assessed by quantitative real-time PCR. $n = 6$ per group.
(E) Flow cytometry analysis of Notch1, VCAM1, P16, and P53 expression in HUVECs.
(F) Quantification of Notch1, VCAM1, P16, and P53. $n = 6$ per group. Data were representative of three independent experiments.
(G) HUVECs were pretreated with IgG or anti-Notch1 mAb at 10 μg/mL for 2 h, then given control exosomes or stroke exosomes (15 μg/mL) for 24 h. THP-1 cells were labeled with fluorescence dye, then cell adhesion assay was performed. Representative images of adhesive cells. Scale bars, 50 μm. $n = 6$ per group. Data were representative of three independent experiments.
(H) HUVECs were pretreated with IgG or anti-VCAM1 mAb (25 μg/mL) for 2 h, then incubated with control exosomes or stroke exosomes (15 μg/mL) for 24 h. THP-1 cells were labeled with fluorescence dye, then cell adhesion assay was performed. Representative images of adhesive cells. Scale bars, 50 μm. $n = 6$ per group. Data were representative of three independent experiments. Mean ± SEM. $^{**}p < 0.01$. Two-tailed unpaired Student's t test (B), two-way ANOVA followed by Tukey post hoc test (D–H).

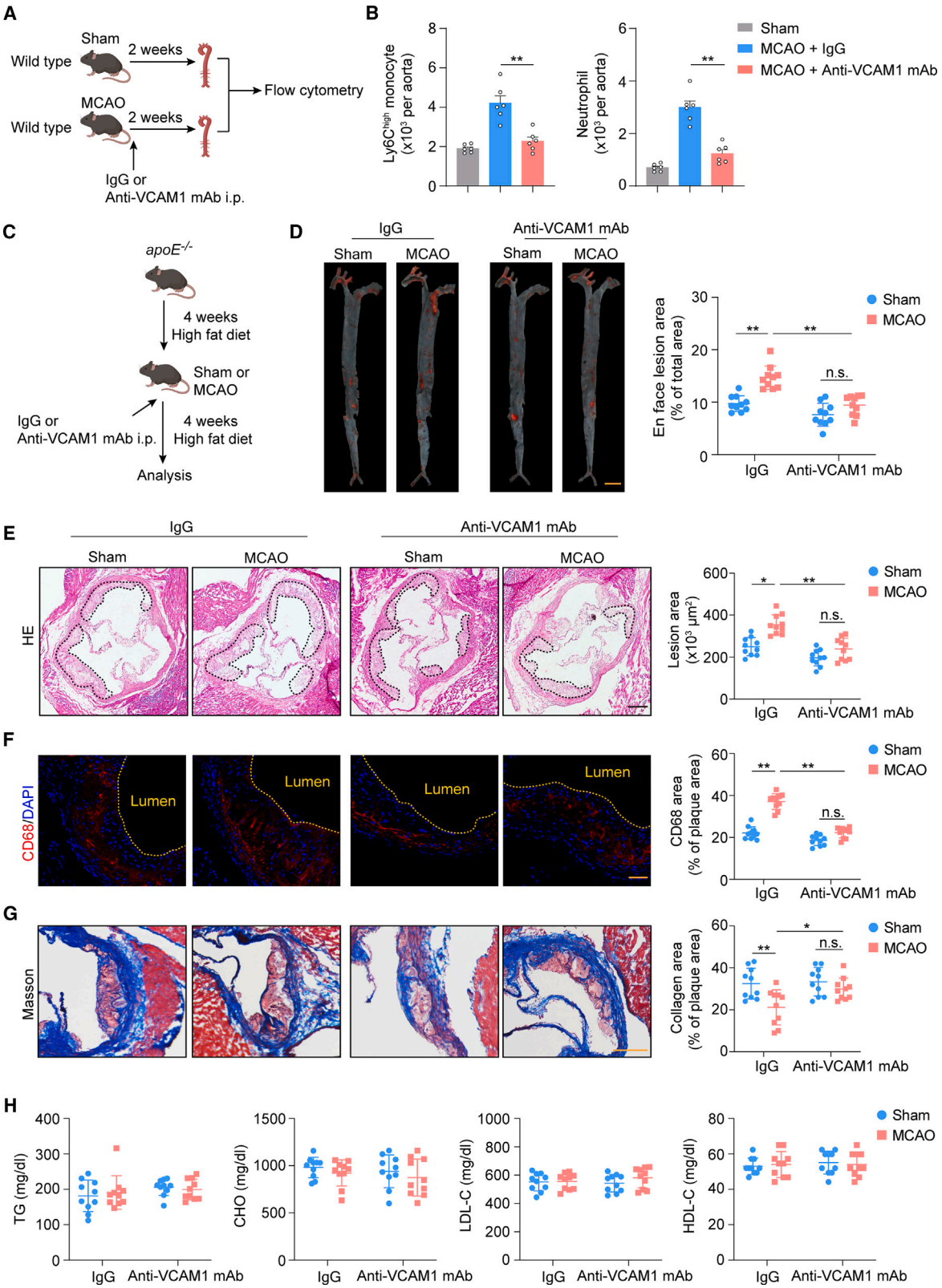

Figure 5. VCAM1 blockade suppresses stroke-induced atheroprogression

(A) Schematic diagram depicts experimental design. Wild-type mice received intraperitoneal (i.p.) injections of IgG control or anti-VCAM1 mAb (5 mg/kg/week) following MCAO surgery. Flow cytometry analysis was conducted at day 14 after surgery.

(legend continued on next page)

were similar in *Tie2Cre-Notch1*$^{fl/-}$*apoE*$^{-/-}$ and *Notch1*$^{fl/-}$*apoE*$^{-/-}$ mice (Figures S5G–S5I).

To assess the effects of ablated microglia DLL1 and Jagged1 on stroke-induced growth of atherosclerotic lesions and vascular inflammation, we generated *Hexb-CreERT2-DLL1/Jagged1*$^{fl/fl}$*apoE*$^{-/-}$ mice and *DLL1/Jagged1*$^{fl/fl}$*apoE*$^{-/-}$ mice. These mice received a high-fat diet for 8 weeks starting from 4 weeks prior to MCAO surgery (Figure S6A). We found that the atherosclerotic lesions were reduced in whole aorta and aortic roots in *Hexb-CreERT2-DLL1/Jagged1*$^{fl/fl}$ *apoE*$^{-/-}$ mice versus *DLL1/Jagged1*$^{fl/fl}$*apoE*$^{-/-}$ mice after stroke, together with a decrease of infiltrating monocytes and oil red O-positive area, and similar collagen content in atherosclerotic plaque (Figures S6B–S6F), whereas no significant difference was noted in *Hexb-CreERT2-DLL1/Jagged1*$^{fl/fl}$*apoE*$^{-/-}$ mice in MCAO group versus sham group (Figures S6B–S6F). We also found a similar αSMA-positive area (Figure S6G). Circulating TG, total CHO, LDL-C, and HDL-C were also similar (Figure S6H). In addition, we found that GW4869 reduced brain ischemia-induced growth of atherosclerotic lesions (Figures S7A–S7D), along with attenuated accumulation of monocytes in atherosclerotic plaque (Figure S7E), similar collagen content and αSMA-positive area (Figures S7F and S7G). In addition, TG, CHO, LDL-C, and HDL-C did not substantially alter in *apoE*$^{-/-}$ MCAO mice receiving GW4869 (Figure S7H).

To test whether Notch1 can be therapeutically targeted to suppress stroke-induced vascular inflammation, we treated wild-type mice with anti-Notch1 mAb for 2 weeks (Figure 7A). Flow cytometry analysis revealed that anti-Notch1 mAb abrogated stroke-induced increase of infiltrating Ly6C^{high} monocytes and neutrophils in aortic tissues at 2 weeks after stroke induction (Figure 7B).

In *apoE*$^{-/-}$ mice receiving anti-Notch1 mAb following MCAO (Figure 7C), we found that anti-Notch1 mAb suppressed brain ischemia-induced growth of atherosclerotic lesions (Figures 7D, 7E, S7I, and S7J), along with attenuated accumulation of macrophages, similar collagen content in atherosclerotic plaques (Figures 7F, 7G, and S7K) and αSMA-positive area (Figures S7L and S7M). Circulating TG, CHO, LDL-C, and HDL-C were not altered in *apoE*$^{-/-}$ MCAO mice receiving anti-Notch1 mAb (Figure 7H). Additionally, treatment with anti-Notch1 mAb did not alter brain infarct size in MCAO mice (Figures S7N and S7O).

Together, these results suggest that disruption of EC Notch1 signaling suppresses atheroprogression following stroke.

DISCUSSION

Our results indicate that acute brain ischemia stimulates a spectrum of adverse events in systemic vasculature including a senescent, pro-inflammatory endothelium with upregulation of VCAM1, which occurs primarily through Notch1 signaling that is switched on by brain-released P2RY12^{+}CX3CR1^{+} exosomes containing Notch1 ligands. These adverse changes at the vascular endothelial surface are persistent to drive myeloid cell adhesion and accelerate plaque growth along with inflammation in peripheral vessels after stroke. Our data also suggest that ablation of vascular Notch1 signaling or inhibition of VCAM1 attenuates adverse endothelial responses in the periphery following stroke.

The identification of persistent EC activation and senescence in the periphery following stroke provides insights into post-stroke atheroprogression. Accumulating evidence suggests that global inflammatory responses after stroke contribute to the evaluated risk for adverse vascular events in the periphery.[12–15] Indeed, leukocytosis and elevated circulating cytokines often occur following stroke, which contribute to the major adverse cardiovascular events and poor prognosis. Carotid activity with ^{18}F-FDG PET has also been found increased in patients with recent ischemic stroke.[16–18] In atherosclerotic mice, acute ischemic stroke has been shown to induce an increase in pro-inflammatory Ly6C^{high} monocytes and other myeloid cells to promote atherosclerosis.[5] However, little is known regarding endothelial changes that promote the recruitment of myeloid cells into atherosclerotic lesions in peripheral vessels after stroke. In this regard, our finding of persistent EC activation and senescence in the peripheral arteries provides additional insight into EC-mediated atheroprogression that contributes to recurrent vascular events following stroke.

This work shows that sustained Notch1 activation in the peripheral vasculature occurs following stroke. This finding is supported by persistent upregulation of EC Notch1 receptor in the periphery and elevated circulating Notch1 ligands in patients with stroke and mice subjected to experimental stroke. As a result, increased Notch1 activity leads to a senescence-like and pro-inflammatory EC phenotype. At a central position to orchestrate leukocyte adhesion and plaque growth in atherosclerosis, ECs express adhesion molecules and produce inflammatory factors to recruit immune cells and direct their infiltration into the atherosclerotic lesions, leading to plaque expansion and rupture that contribute to recurrent vascular events. Notably, we found that P2RY12^{+}CX3CR1^{+} exosomes carried Notch1 ligands to activate EC Notch1 in the periphery. In line with our findings, recent studies indicated that ischemic brain can release alarmins such as HMGB1 to mobilize monocytes and accelerate atheroprogression, suggesting a critical role of brain-derived factors to orchestrate remote vascular response after stroke.[5,19,20] Indeed, we found an increase in circulating HMGB1 after brain

(B) Counts of Ly6C^{high} monocytes (left) and neutrophils (right) in aorta. n = 6 mice per group. Data were representative of three independent experiments.
(C) High-fat-diet-fed *apoE*$^{-/-}$ mice received IgG or anti-VCAM1 mAb (5 mg/kg/week) following MCAO surgery and were sacrificed 4 weeks later.
(D) Oil red O staining of aortas. Scale bars, 4 mm. n = 10 mice per group. Data were representative of four independent experiments.
(E) H&E-stained cross sections at the aortic root. Black dashed lines demarcate atherosclerotic plaque. n = 10 mice per group. Data were representative of four independent experiments. Scale bars, 250 μm.
(F) CD68-positive staining. n = 10 mice per group. Data were representative of four independent experiments. Scale bars, 50 μm.
(G) Masson staining (left), quantification of plaque collagen area versus plaque area (right). n = 10 mice per group. Data were representative of four independent experiments. Scale bars, 250 μm.
(H) Circulating TG, CHO, LDL-C, and HDL-C. n = 10 mice per group. Data were representative of four independent experiments. Mean ± SEM. *p < 0.05, **p < 0.01. n.s., not significant. One-way ANOVA followed by Tukey post hoc test. (B) two-way ANOVA followed by Tukey post hoc test (D–G).
See also Figure S4.

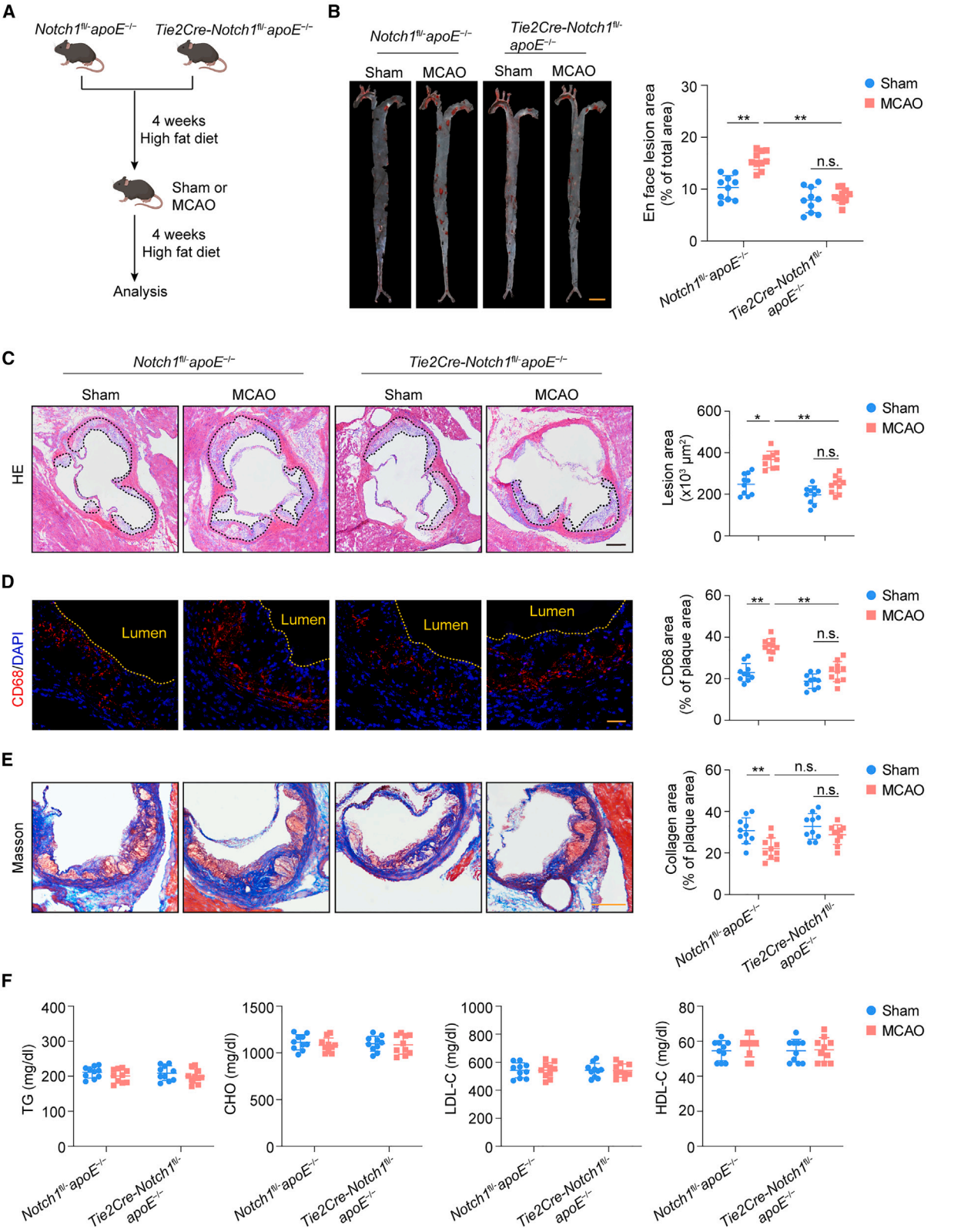

Figure 6. Disruption of endothelial Notch1 attenuates stroke-induced atheroprogression

(A) Schematic diagram depicts experimental design. High-fat-diet *Notch1*$^{fl/-}$*apoE*$^{-/-}$ and *Tie2Cre- Notch1*$^{fl/-}$*apoE*$^{-/-}$ mice underwent MCAO surgery and were sacrificed 4 weeks later.

(legend continued on next page)

ischemia. Of note, the expression of *Ager* (receptor of HMGB1) was not substantially altered in MCAO mice versus sham controls. These results imply that stroke-induced activation of ECs may not rely on post-ischemic release of HMGB1.

Our identification of P2RY12^{+}CX3CR1^{+} cells-derived exosomal Notch 1 ligands DLL1 and Jagged1 suggests exosomes as a critical carrier of molecules that act primarily on ECs throughout the body after brain ischemia. The pivotal role of microglia in the control of systemic vascular response is at least partially supported by one recent study showing that microglia contribute to the elevated blood pressure in hypertension animals, in which such process may involve local inflammatory factors tumor necrosis factor alpha (TNF-α)_ and interleukin-1β (IL-1β) derived from microglia.[21–23]

Using combined approaches of flow cytometry, pathology, and imaging, we found that stroke induces remote arterial upregulation of EC adhesion molecules that persistently recruit inflammatory cells. Although our major measurements were confined to large arteries in the periphery, these adverse events may also include other vascular territories including medium and small vessels. As such, it is reasonable to postulate that brain ischemia promotes global endothelial activation. We believe that endothelial activation was at least partially responsible for the acceleration of plaque growth, inflammation, and necrotic core at weeks to months post-stroke, which could be consistent with high-risk plaque appearance on histology. Given the multifactorial role of monocytes in promoting plaque inflammation, there is a possibility that increased plaque monocytes may partially contribute to the persistence of endothelial activation in atherosclerotic mice. However, it is noteworthy that monocytes in the periphery have minimal expression of Notch1 ligands. Additionally, conditional knockdown of EC Notch1 or blockade of Notch1 signaling was sufficient to reduce post-stroke atheroprogression, which suggests a central role of upregulated EC Notch1 activity in the acceleration of atherosclerosis and adverse vascular events after brain ischemia.

Notch1 activation can switch on gene expression of cyclin-dependent kinases to induce cellular senescence. As a reaction to stress, senescence results in cell-cycle arrest in the presence of mitogens, high metabolic rate, expression of molecular effectors (e.g., p16, p21, and p53), inflammatory cytokines, adhesion molecules such as VCAM1, and classical markers such as senescence-associated β-gal.[24–26] Our experiments indicate that sustained Notch1 activity in ECs induces a senescence-like phenotype that facilitates leukocyte adhesion and vascular inflammation. As an adhesion factor for leukocytes, VCAM1 also transmits signals into the EC, leading to stress fiber formation, endothelial stiffening, and vascular aging.[27–29] VLA-4, i.e., α4β1-integrin ligand, expression on leukocytes may facilitate binding of VCAM1 on activated ECs.[30] As such, interference with VCAM1 binding, e.g., by the α4-integrin blocking mAb, has been used to prevent Notch1 activation-induced increase in neutrophil infiltration.[31–33] Consistent with these findings, we showed that antibody blockade of Notch1 activation or α4-integrin reduced monocyte infiltration and plaque groups in atherosclerotic mice after stroke. Obviously, these antibodies target not only ECs but also several other cell types. Nevertheless, the efficacy of these treatments to reduce plaque growth after stroke, together with the results from conditional mutants showing the contribution of EC Notch1 to atheroprogression, implies the potential of these treatments to attenuate stroke-induced acceleration of atherosclerosis. In all, our data characterize Notch signaling activation in the vasculature as a risk factor for adverse vascular events after stroke that can be therapeutically targeted.

In summary, stroke leads to systemic endothelial activation and upregulation of EC adhesive molecules. These processes lead to enhanced monocyte recruitment and adhesion to ECs to accelerate post-stroke plaque progression. Disruption of EC Notch1 activation or VCAM1-mediated leukocyte adhesion suppresses these adverse systemic EC changes. Our findings reveal mechanisms underlying the heightened risk for recurrent vascular events after stroke and identify modifiable processes that may serve as potential therapeutic targets.

Limitations of the study

The major finding of this work highlights Notch1 hyperactivation in endothelium that augments myeloid cell adhesion and atheroprogression following stroke. Although we found increased circulating Notch1 ligands in patients with ischemic stroke, the clinical relevance of this finding to stroke recurrence awaits further investigation in a large cohort of stroke patients. We found that microglia were likely a major source of exosomal Notch 1 ligands. The precise markers are needed to pinpoint out the exact contribution from microglia in future studies. Additionally, stroke induces the release of various alarmins that are not limited to HMGB1, and these alarmins contribute to atheroprogression after stroke; stroke-induced EC activation may involve other components of alarmins. Future investigations are required to sort out these signals that may profoundly affect EC health and immune activation.

STAR★METHODS

Detailed methods are provided in the online version of this paper and include the following:

- KEY RESOURCES TABLE
- RESOURCE AVAILABILITY

(B) Oil red O staining of aortas. Scale bars, 4 mm. n = 10 mice per group.
(C) H&E-stained cross sections at the aortic root. Black dashed lines demarcate atherosclerotic plaque. n = 10 mice per group. Data were representative of four independent experiments. Scale bars, 250 μm.
(D) CD68-positive staining. n = 10 mice per group. Data were representative of four independent experiments. Scale bars, 50 μm.
(E) Masson staining (left), quantification of plaque collagen area versus plaque area (right). n = 10 mice per group. Data were representative of four independent experiments. Scale bars, 250 μm.
(F) Circulating TG, total CHO, LDL-C, and HDL-C. n = 10 mice per group. Data were representative of four independent experiments. Mean ± SEM. $^{*}p < 0.05$, $^{**}p < 0.01$. n.s., not significant. Two-way ANOVA followed by Tukey post hoc test (B–E).
See also Figures S5–S7.

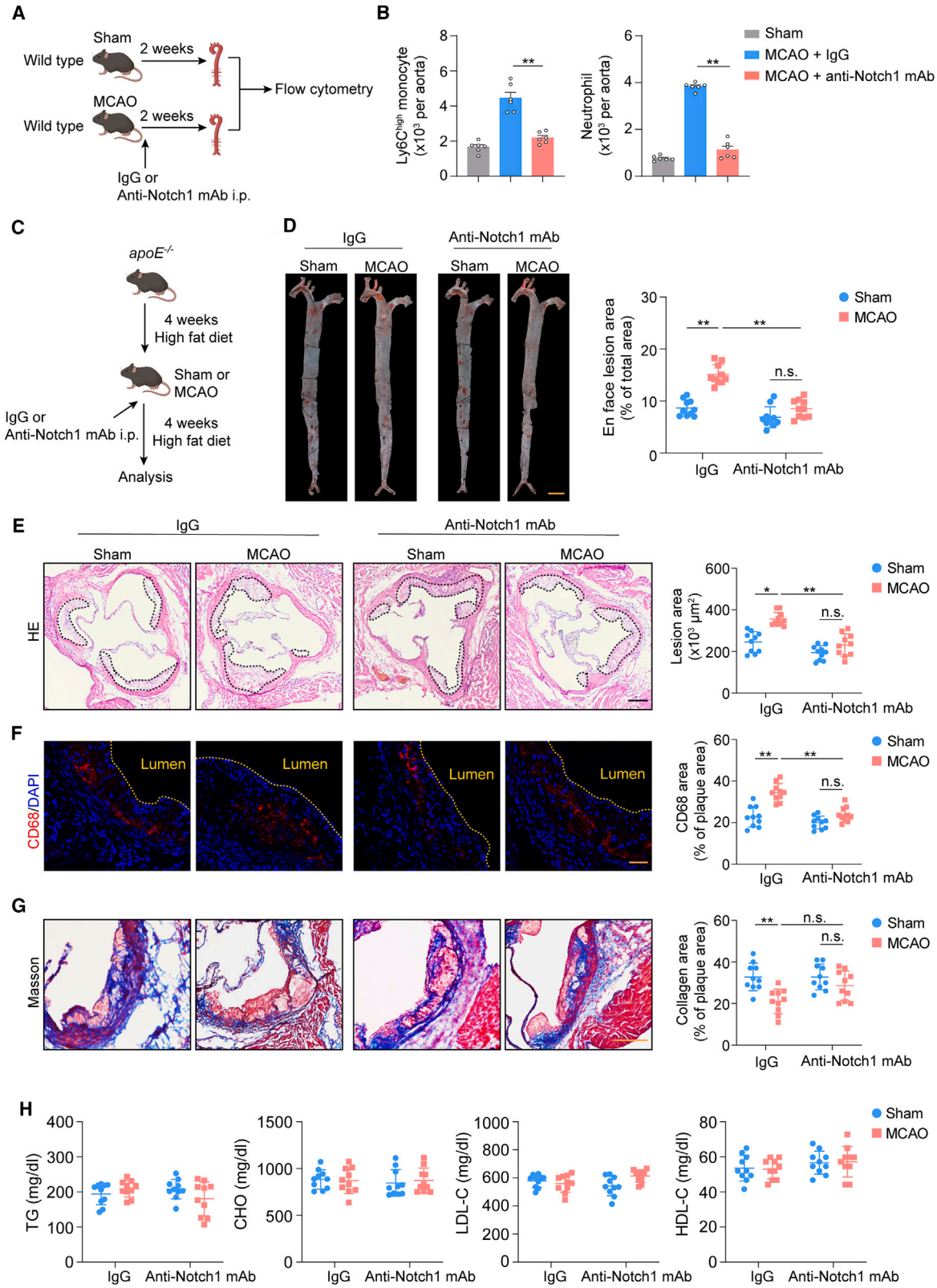

Figure 7. Notch1 blockade alleviates stroke-induced atheroprogression

(A) Schematic diagram depicts experimental design. Wild-type mice were received i.p. injections of IgG control or anti-Notch1 (5 mg/kg/week) underwent MCAO surgery. Flow cytometry analysis was conducted at day 14 after surgery.

(legend continued on next page)

SUPPLEMENTAL INFORMATION

Supplemental information can be found online at https://doi.org/10.1016/j.immuni.2024.07.002.

ACKNOWLEDGMENTS

This work was supported in part by the National Science Foundation of China (82225015, 82171284, 82200279, 81925018, and 82130049), the National Key Research and Development Project of China (2022YFC2502401 and 2021ZD0202400), the New Cornerstone Science Foundation through the XPLORER PRIZE, the National Postdoctoral Program for Innovative Talents (BX20220227), the Postdoctoral Science Foundation (2022M712390), the Science and Technology Development Fund of Tianjin Education Commission for higher education grant (2021ZD035), and the Tianjin Key Medical Discipline (Specialty) Construction Project.

AUTHOR CONTRIBUTIONS

Q.L. formulated the concept and designed the studies. M.L. designed the studies and performed the experiments. D.W., J.S., L.L., H.X., and H.R. performed the experiments. M.L, C.Q., Z.L., and M.Z. analyzed the results. M.L., C.Q., D.W., J.Z., D.A., and Q.L. interpreted the results. M.L., J.Z., D.A., Q.Z., and Q.L. wrote and edited the manuscript.

DECLARATION OF INTERESTS

The authors declare no competing interests.

Received: November 28, 2023
Revised: March 31, 2024
Accepted: July 3, 2024
Published: July 29, 2024

REFERENCES

1. Burn, J., Dennis, M., Bamford, J., Sandercock, P., Wade, D., and Warlow, C. (1994). Long-term risk of recurrent stroke after a first-ever stroke. The Oxfordshire Community Stroke Project. Stroke *25*, 333–337.
2. Uzuner, N., and Uzuner, G.T. (2023). Risk factors for multiple recurrent ischemic strokes. Brain Circ. *9*, 21–24.
3. Tu, W.J., Zhao, Z., Yin, P., Cao, L., Zeng, J., Chen, H., Fan, D., Fang, Q., Gao, P., Gu, Y., et al. (2023). Estimated Burden of Stroke in China in 2020. JAMA Netw. Open *6*, e231455.
4. Li, L., Poon, M.T.C., Samarasekera, N.E., Perry, L.A., Moullaali, T.J., Rodrigues, M.A., Loan, J.J.M., Stephen, J., Lerpiniere, C., Tuna, M.A., et al. (2021). Risks of recurrent stroke and all serious vascular events after spontaneous intracerebral haemorrhage: pooled analyses of two population-based studies. Lancet Neurol. *20*, 437–447.
5. Roth, S., Singh, V., Tiedt, S., Schindler, L., Huber, G., Geerlof, A., Antoine, D.J., Anfray, A., Orset, C., Gauberti, M., et al. (2018). Brain-released alarmins and stress response synergize in accelerating atherosclerosis progression after stroke. Sci. Transl. Med. *10*, eaao1313.
6. Davignon, J., and Ganz, P. (2004). Role of Endothelial Dysfunction in Atherosclerosis. Circulation *109*, III27–III32.
7. Wang, Y., Jing, J., Meng, X., Pan, Y., Wang, Y., Zhao, X., Lin, J., Li, W., Jiang, Y., Li, Z., et al. (2019). The Third China National Stroke Registry (CNSR-III) for patients with acute ischaemic stroke or transient ischaemic attack: design, rationale and baseline patient characteristics. Stroke Vasc. Neurol. *4*, 158–164.
8. Zhou, B., Lin, W., Long, Y., Yang, Y., Zhang, H., Wu, K., and Chu, Q. (2022). Notch signaling pathway: architecture, disease, and therapeutics. Signal Transduct. Target. Ther. *7*, 95.
9. Hassan, W.A., Yoshida, R., Kudoh, S., Hasegawa, K., Niimori-Kita, K., and Ito, T. (2014). Notch1 controls cell invasion and metastasis in small cell lung carcinoma cell lines. Lung Cancer *86*, 304–310.
10. Kopan, R., and Ilagan, M.X.G. (2009). The canonical Notch signaling pathway: unfolding the activation mechanism. Cell *137*, 216–233.
11. Sheldon, H., Heikamp, E., Turley, H., Dragovic, R., Thomas, P., Oon, C.E., Leek, R., Edelmann, M., Kessler, B., Sainson, R.C.A., et al. (2010). New mechanism for Notch signaling to endothelium at a distance by Delta-like 4 incorporation into exosomes. Blood *116*, 2385–2394.

(B) Counts of Ly6C^{high} monocytes (right) and neutrophils (left) in aorta. n = 6 mice per group. Data were representative of three independent experiments.
(C) Schematic diagram depicts experimental design. High-fat-diet-fed *apoE*$^{-/-}$ mice received IgG or anti-Notch1 mAb (5 mg/kg/week) underwent MCAO surgery and were sacrificed 4 weeks later.
(D) Oil red O staining of aortas. Scale bars, 4 mm. n = 10 mice per group. Data were representative of four independent experiments.
(E) H&E-stained cross sections at the aortic root. Black dashed lines demarcate atherosclerotic plaque. n = 10 mice per group. Data were representative of four independent experiments. Scale bars, 250 μm.
(F) CD68-positive staining. n = 10 mice per group. Data were representative of four independent experiments. Scale bars, 50 μm.
(G) Masson staining (left), quantification of plaque collagen area versus plaque area (right). n = 10 mice per group. Data were representative of four independent experiments. Scale bars, 250 μm.
(H) Circulating TG, total CHO, LDL-C, and HDL-C. n = 10 mice per group. Data were representative of four independent experiments. Mean ± SEM. $^{*}p < 0.05$, $^{**}p < 0.01$. n.s., not significant. One-way ANOVA followed by Tukey post hoc test (B), two-way ANOVA followed by Tukey post hoc test (D–G).
See also Figure S7.

12. Gerhard, A., Schwarz, J., Myers, R., Wise, R., and Banati, R.B. (2005). Evolution of microglial activation in patients after ischemic stroke: a [11C](R)-PK11195 PET study. Neuroimage *24*, 591–595.

13. Price, C.J.S., Wang, D., Menon, D.K., Guadagno, J.V., Cleij, M., Fryer, T., Aigbirhio, F., Baron, J.C., and Warburton, E.A. (2006). Intrinsic activated microglia map to the peri-infarct zone in the subacute phase of ischemic stroke. Stroke *37*, 1749–1753.

14. Radlinska, B.A., Ghinani, S.A., Lyon, P., Jolly, D., Soucy, J.P., Minuk, J., Schirrmacher, R., and Thiel, A. (2009). Multimodal microglia imaging of fiber tracts in acute subcortical stroke. Ann. Neurol. *66*, 825–832.

15. Thiel, A., Radlinska, B.A., Paquette, C., Sidel, M., Soucy, J.P., Schirrmacher, R., and Minuk, J. (2010). The temporal dynamics of poststroke neuroinflammation: a longitudinal diffusion tensor imaging-guided PET study with 11C-PK11195 in acute subcortical stroke. J. Nucl. Med. *51*, 1404–1412.

16. Chaker, S., Al-Dasuqi, K., Baradaran, H., Demetres, M., Delgado, D., Nehmeh, S., Osborne, J.R., Christos, P.J., Kamel, H., and Gupta, A. (2019). Carotid Plaque Positron Emission Tomography Imaging and Cerebral Ischemic Disease. Stroke *50*, 2072–2079.

17. Kwee, R.M., Truijman, M.T., Mess, W.H., Teule, G.J., ter Berg, J.W., Franke, C.L., Korten, A.G., Meems, B.J., Prins, M.H., van Engelshoven, J.M., et al. (2011). Potential of integrated [18F] fluorodeoxyglucose positron-emission tomography/CT in identifying vulnerable carotid plaques. AJNR Am. J. Neuroradiol. *32*, 950–954.

18. Kelly, P.J., Camps-Renom, P., Giannotti, N., Martí-Fàbregas, J., Murphy, S., McNulty, J., Barry, M., Barry, P., Calvet, D., Coutts, S.B., et al. (2019). Carotid Plaque Inflammation Imaged by (18)F-Fluorodeoxyglucose Positron Emission Tomography and Risk of Early Recurrent Stroke. Stroke *50*, 1766–1773.

19. Qiu, J., Xu, J., Zheng, Y., Wei, Y., Zhu, X., Lo, E.H., Moskowitz, M.A., and Sims, J.R. (2010). High-mobility group box 1 promotes metalloproteinase-9 upregulation through toll-like receptor 4 after cerebral ischemia. Stroke *41*, 2077–2082.

20. Pais, T.F., Ali, H., Moreira da Silva, J., Duarte, N., Neres, R., Chhatbar, C., Acúrcio, R.C., Guedes, R.C., Strano Moraes, M.C., Costa-Silva, B., et al. (2022). Brain endothelial STING1 activation by Plasmodium-sequestered heme promotes cerebral malaria via type I IFN response. Proc. Natl. Acad. Sci. USA *119*, e2206327119.

21. Shen, X.Z., Li, Y., Li, L., Shah, K.H., Bernstein, K.E., Lyden, P., and Shi, P. (2015). Microglia participate in neurogenic regulation of hypertension. Hypertension *66*, 309–316.

22. Calvillo, L., Gironacci, M.M., Crotti, L., Meroni, P.L., and Parati, G. (2019). Neuroimmune crosstalk in the pathophysiology of hypertension. Nat. Rev. Cardiol. *16*, 476–490.

23. Touyz, R.M., and Camargo, L.L. (2019). Microglia, the Missing Link in the Brain-Gut-Hypertension Axis. Circ. Res. *124*, 671–673.

24. Wieland, E., Rodriguez-Vita, J., Liebler, S.S., Mogler, C., Moll, I., Herberich, S.E., Espinet, E., Herpel, E., Menuchin, A., Chang-Claude, J., et al. (2017). Endothelial Notch1 Activity Facilitates Metastasis. Cancer Cell *31*, 355–367.

25. Parry, A.J., Hoare, M., Bihary, D., Hänsel-Hertsch, R., Smith, S., Tomimatsu, K., Mannion, E., Smith, A., D'Santos, P., Russell, I.A., et al. (2018). NOTCH-mediated non-cell autonomous regulation of chromatin structure during senescence. Nat. Commun. *9*, 1840.

26. Teo, Y.V., Rattanavirotkul, N., Olova, N., Salzano, A., Quintanilla, A., Tarrats, N., Kiourtis, C., Müller, M., Green, A.R., Adams, P.D., et al. (2019). Notch Signaling Mediates Secondary Senescence. Cell Rep. *27*, 997–1007.e5.

27. Yousef, H., Czupalla, C.J., Lee, D., Chen, M.B., Burke, A.N., Zera, K.A., Zandstra, J., Berber, E., Lehallier, B., Mathur, V., et al. (2019). Aged blood impairs hippocampal neural precursor activity and activates microglia via brain endothelial cell VCAM1. Nat. Med. *25*, 988–1000.

28. Bhatia, K., Ahmad, S., Kindelin, A., and Ducruet, A.F. (2021). Complement C3a receptor-mediated vascular dysfunction: a complex interplay between aging and neurodegeneration. J. Clin. Invest. *131*, e144348.

29. Bordon, Y. (2019). Targeting VCAM1 rejuvenates the brain in aged mice. Nat. Rev. Immunol. *19*, 415.

30. Peng, Z., Shu, B., Zhang, Y., and Wang, M. (2019). Endothelial Response to Pathophysiological Stress. Arterioscler. Thromb. Vasc. Biol. *39*, e233–e243.

31. Pinho, S., Wei, Q., Maryanovich, M., Zhang, D., Balandrán, J.C., Pierce, H., Nakahara, F., Di Staulo, A., Bartholdy, B.A., Xu, J., et al. (2022). VCAM1 confers innate immune tolerance on haematopoietic and leukaemic stem cells. Nat. Cell Biol. *24*, 290–298.

32. Vajkoczy, P., Laschinger, M., and Engelhardt, B. (2001). Alpha4-integrin-VCAM-1 binding mediates G protein-independent capture of encephalitogenic T cell blasts to CNS white matter microvessels. J. Clin. Invest. *108*, 557–565.

33. Bowden, R.A., Ding, Z.M., Donnachie, E.M., Petersen, T.K., Michael, L.H., Ballantyne, C.M., and Burns, A.R. (2002). Role of alpha4 integrin and VCAM-1 in CD18-independent neutrophil migration across mouse cardiac endothelium. Circ. Res. *90*, 562–569.

34. He, J., Bao, Q., Zhang, Y., Liu, M., Lv, H., Liu, Y., Yao, L., Li, B., Zhang, C., He, S., et al. (2018). Yes-Associated Protein Promotes Angiogenesis via Signal Transducer and Activator of Transcription 3 in Endothelial Cells. Circ. Res. *122*, 591–605.

35. Wang, J.M., Chen, A.F., and Zhang, K. (2016). Isolation and Primary Culture of Mouse Aortic Endothelial Cells. J. Vis. Exp. *118*, 52965.

36. Foteinos, G., Hu, Y., Xiao, Q., Metzler, B., and Xu, Q. (2008). Rapid endothelial turnover in atherosclerosis-prone areas coincides with stem cell repair in apolipoprotein E-deficient mice. Circulation *117*, 1856–1863.

37. Liu, Q., Jin, W.N., Liu, Y., Shi, K., Sun, H., Zhang, F., Zhang, C., Gonzales, R.J., Sheth, K.N., La Cava, A., and Shi, F.D. (2017). Brain Ischemia Suppresses Immunity in the Periphery and Brain via Different Neurogenic Innervations. Immunity *46*, 474–487.

38. Gan, Y., Liu, Q., Wu, W., Yin, J.X., Bai, X.F., Shen, R., Wang, Y., Chen, J., La Cava, A., Poursine-Laurent, J., et al. (2014). Ischemic neurons recruit natural killer cells that accelerate brain infarction. Proc. Natl. Acad. Sci. USA *111*, 2704–2709.

39. Shi, K., Li, H., Chang, T., He, W., Kong, Y., Qi, C., Li, R., Huang, H., Zhu, Z., Zheng, P., et al. (2022). Bone marrow hematopoiesis drives multiple sclerosis progression. Cell *185*, 2234–2247.e17.

40. He, L., Fu, Y., Deng, J., Shen, Y., Wang, Y., Yu, F., Xie, N., Chen, Z., Hong, T., Peng, X., et al. (2018). Deficiency of FAM3D (Family With Sequence Similarity 3, Member D), A Novel Chemokine, Attenuates Neutrophil Recruitment and Ameliorates Abdominal Aortic Aneurysm Development. Arterioscler. Thromb. Vasc. Biol. *38*, 1616–1631.

41. Li, H.D., Li, R., Kong, Y., Zhang, W., Qi, C., Wang, D., Hao, H., and Liu, Q. (2022). Selective Sphingosine 1-Phosphate Receptor 1 Modulation Augments Thrombolysis of Low-Dose Tissue Plasminogen Activator Following Cerebrovascular Thrombosis. Front. Immunol. *13*, 801727.

42. Chen, G., Huang, A.C., Zhang, W., Zhang, G., Wu, M., Xu, W., Yu, Z., Yang, J., Wang, B., Sun, H., et al. (2018). Exosomal PD-L1 contributes to immunosuppression and is associated with anti-PD-1 response. Nature *560*, 382–386.

43. Shi, S.X., Shi, K., and Liu, Q. (2021). Brain injury instructs bone marrow cellular lineage destination to reduce neuroinflammation. Sci. Transl. Med. *13*, eabc7029.

44. Jin, W.N., Shi, K., He, W., Sun, J.H., Van Kaer, L., Shi, F.D., and Liu, Q. (2021). Neuroblast senescence in the aged brain augments natural killer cell cytotoxicity leading to impaired neurogenesis and cognition. Nat. Neurosci. *24*, 61–73.

STAR★METHODS

KEY RESOURCES TABLE

REAGENTS or RESOURCES	SOURCE	IDENTIFIER
Antibodies		
PerCP/Cyanine5.5 anti-mouse CD45	Biolegend	Cat #103132; RRID: AB_893340
APC anti-mouse CD31	Biolegend	Cat #102410; RRID: AB_312904
APC/Cyanine7 anti-mouse CD45	Biolegend	Cat #157204; RRID: AB_2876533
PE/Cyanine7 anti-mouse CD106	Biolegend	Cat #105720; RRID: AB_2214047
PE anti-Notch 1	Biolegend	Cat #629106; RRID: AB_2251468
p53 (DO-1)	Santa Cruz Biotechnology	Cat #sc-126; RRID: AB_628082
CDKN2B/CDKN2A/p16 (C-7)	Santa Cruz Biotechnology	Cat #sc-377412; RRID: AB_2936231
FITC anti-mouse/human CD11b	Biolegend	Cat #101206; RRID: AB_312788
PE anti-mouse DLL1	Biolegend	Cat #128307; RRID: AB_1133995
APC anti-mouse CD339 (Jagged 1)	Biolegend	Cat #130914; RRID: AB_2561305
FITC anti-mouse CX3CR1	Biolegend	Cat #149020; RRID: AB_2565702
BV510 anti-human CD171	BD Biosciences	Cat #750559; RRID: AB_2874696
GFAP (GA5) mouse mAb	Cell Signaling Technology	Cat #3655; RRID: AB_2263284
Jagged1 (D4Y1R) rabbit mAb	Cell Signaling Technology	Cat #54340; RRID: AB_2799457
APC/Cyanine7 anti-human CD63	Biolegend	Cat #353046; RRID: AB_2860922
CD171 (L1-CAM)-APC	Miltenyi	Cat #130-102-221; RRID: AB_2655594
Alexa Fluor 647 anti-P2RY12	Biolegend	Cat #848018; RRID: AB_2941635
PE anti-mouse Ly-6G/Ly-6C (Gr-1)	Biolegend	Cat #108408; RRID: AB_313373
Mouse Monoclonal CD63 (MX-49.129.5)	Novus	Cat #NBP2-34689PCP; RRID: AB_3107056
PE anti-human DLL1	Biolegend	Cat #346404; RRID: AB_2277361
APC anti-human CD63	Biolegend	Cat # 353008; RRID: AB_10916521
BV421 anti-human P2RY12	Biolegend	Cat # 392106; RRID: AB_2783291
Anti-CD68 (KP1)	Abcam	Cat #ab955; RRID: AB_307338
Anti-αSMA	Sigma-Aldrich	Cat #A5228; RRID: AB_262054
Cleaved Notch1 (Val1744) (D3B8)	Cell Signaling Technology	Cat #4147; RRID: AB_2153348
FITC anti-human CX3CR1	Biolegend	Cat #341606; RRID: AB_1626276
Biological Samples		
Human plasma	Tianjin Medical University General Hospital	N/A
Chemicals, Peptides, and Recombinant Proteins		
Anti-VCAM1	Sigma-Aldrich	Cat #CBL1300
Anti- Notch 1	Biolegend	Cat #352112
Mouse IgG1κ	MedChemExpress	Cat #HY-P99977
GW4869	MedChemExpress	Cat #HY-19363
Tamoxifen	Sigma-Aldrich	Cat #T5648
Percoll	Thermo Fisher Scientific	Cat #45-001-747
CellTrace calcein red-orange AM	Thermo Fisher Scientific	Cat #C34851
Dextran, oregon green 488	Thermo Fisher Scientific	Cat #D7172
CellTrace™ CFSE	Thermo Fisher Scientific	Cat #C34554
Papain	Absin	Cat #abs47014927
DNase I	Sigma-Aldrich	Cat #D5025
Collagenase type I	Thermo Fisher Scientific	Cat #17100017
JSH-23	MedChemExpress	Cat #HY-13982
RIPA buffer	Solarbio	Cat #R0010

(*Continued on next page*)

Continued

REAGENTS or RESOURCES	SOURCE	IDENTIFIER
Cocktail	Roche	Cat #04693132001
PhosSTOP	Roche	Cat #04906845001
Critical commercial assays		
CellEvent™ senescence green	Thermo Fisher Scientific	Cat #C10840
Total exosome isolation kit	Thermo Fisher Scientific	Cat #4484450
Cytofix/Cytoperm fixation/permeabilization kit	BD Biosciences	Cat #554715
Mouse DLL1 elisa kit	FineTest	Cat #EM6642
Mouse DLL3 elisa kit	FineTest	Cat #EM2010
Mouse DLL4 elisa kit	FineTest	Cat #EM2011
Mouse Jagged1 elisa kit	FineTest	Cat #EM1918
Mouse Jagged2 elisa kit	FineTest	Cat #EM7320
Mouse HMGB1 elisa kit	FineTest	Cat #EM0382
Human Jagged1 elisa kit	FineTest	Cat #EH4500
Human DLL1 elisa kit	FineTest	Cat #EH0115
EasyPure RNA Kit	TransGen Biotech	Cat #ER101-01
SuperScript III and random primers	Thermo Fisher Scientific	Cat #12574035
TransStart Top Green qPCR SuperMix	TransGen Biotech	Cat #AQ131-01
CHO	BioSino Bio-Technology and Science	Cat #20162400910
TG	BioSino Bio-Technology and Science	Cat #20162400911
LDL-C	BioSino Bio-Technology and Science	Cat #20162400518
HDL-C	BioSino Bio-Technology and Science	Cat #20162400513
Deposited data		
Mouse aortic endothelial cells single cell RNA-sequencing	This paper	GSA: OMIX004668 https://ngdc.cncb.ac.cn/omix/
Experimental Models: Cell Lines		
THP-1	ATCC	Cat #TIB-202
Experimental models: Organisms/strains		
Mouse: Wild type (C57BL/6J)	Vital River Laboratory Animal Technology	Cat #Jackson 000664; RRID: IMSR_JAX:000664
Mouse: *apoE*$^{-/-}$	Vital River Laboratory Animal Technology	Cat #Jackson 002052; RRID: IMSR_JAX:000664
Mouse: C57BL/6-*Notch1*$^{fl/-}$	Cyagen Biosciences Inc	N/A
Mouse: C57BL/6-*Tie2-Cre*	Cyagen Biosciences Inc	N/A
Mouse: C57BL/6-*Hexb-CreERT2*	Shanghai Model Organisms Center	N/A
Mouse: C57BL/6-*DLL1*$^{fl/fl}$*Jagged1*$^{fl/fl}$	Cyagen Biosciences Inc	N/A
Oligonucleotides		
Primers for *β-actin* Forward: CATGTACG TTGCTATCCAGGC Reverse: CTCCTTAATGTCACGCACGAT	This paper	N/A
Primers for *VCAM1* Forward: TTTGACAG GCTGGAGATAGACT Reverse: TCAATGTGTAATTTAGCTCGGCA	This paper	N/A
Primers for *Notch1* Forward: CGCTGACGG AGTACAAGTG Reverse: GTAGGAGCCGACCTCGTTG	This paper	N/A

(*Continued on next page*)

Continued

REAGENTS or RESOURCES	SOURCE	IDENTIFIER
Primers for *Notch2* Forward: ATGTGGACG AGTGTCTGTTGC Reverse: GGAAGCATAGGCACAGTCATC	This paper	N/A
Primers for *Notch3* Forward: TGCCAGAG TTCAGTGGTGG Reverse: CACAGGCAAATCGGCCATC	This paper	N/A
Primers for *Notch4* Forward: CTCTTGCCA CTCAATTTCCCT Reverse: TTGCAGAGTTGGGTATCCCTG	This paper	N/A
Primers for *P53* Forward: GAGGTTGGCT CTGACTGTACC Reverse: TCCGTCCCAGTAGATTACCAC	This paper	N/A
Primers for *P16* Forward: GGGTTTTCGT GGTTCACATCC Reverse: CTAGACGCTGGCTCCTCAGTA	This paper	N/A
Software and Algorithms		
Image J	NIH Image	https://imagej.en.softonic.com/
Image-Pro	NIH Image	https://imagej.nih.gov/ij
FlowJo™ v10	Tree Star	https://www.flowjo.com/solutions/flowjo/downloads
Prism 9	GraphPad	https://www.graphpad.com/scientificsoftware/prism/
Online heat map generator	Morpheus	https://software.broadinstitute.org/morpheus/
Graphical design software	BioRender	https://biorender.com/

RESOURCE AVAILABILITY

Lead contact

Further information and requests for resources and reagents should be directed to and will be fulfilled by the lead contact, Qiang Liu (qliu@tmu.edu.cn).

Materials availability

All mouse lines are available from the lead contact with a completed Materials Transfer Agreement.

Data and code availability

- The single cell RNA-sequencing datasets generated during this study have been deposited at Genome Sequence Archive (GSA) and are publically available from the date of publication. Accession numbers are listed in the key resources table.
- This paper does not report original code.
- Any additional information required to reanalyze the data reported in this paper is available from the lead contact upon request.

EXPERIMENTAL MODEL AND SUBJECT DETAILS

Human plasma samples

Patient studies were conducted in accordance with the Declaration of Helsinki. The inclusion of human subjects and supporting documentation was approved by the Ethics Committees of Tianjin Medical University General Hospital (protocol approval number: IRB2022-YX-277-01). Informed consent was obtained from all subjects at the time of enrollment. Human plasma samples were obtained from patients with ischemic stroke at 1 day and 14 day (23 male, 8 female). Human plasma samples of healthy individuals were used as controls (9 male, 8 female). There was no significant statistical difference regarding the age of recruited subjects (Ischemic stroke patients vs. Controls: 66.8 ±7.8 vs. 65.4 ± 4.2 years, P = 0.589). Inclusion criteria for patients with ischemic stroke patients older than 18 years of age. Exclusion criteria include acute myocardial infarction, heart failure, liver diseases (liver cirrhosis, fatty liver and viral hepatitis etc.), autoimmune diseases, preexisting brain diseases, and infections, and concomitant use of immunosuppressive or immune-modulating therapies. Inclusion criteria for healthy controls: 1) Subjects older than 18 years of age; 2) Generally healthy, Body Mass Index between 18-34 and normal basic laboratory tests. Demographics provided in Table S1.

Mice

Wild type (WT) mice and *apoE*$^{-/-}$ mice were purchased from Beijing Vital River Laboratory Animal Technology (Beijing, China). Notch1-knockout-floxed (*Notch1*$^{fl/-}$) and *Tie2-Cre* mice were purchased from Cyagen Biosciences Inc. DLL1-knockout-floxed (*DLL1*$^{fl/fl}$) and Jagged1-knockout-floxed (*Jagged1*$^{fl/fl}$) were purchased from Cyagen Biosciences Inc. *Hexb-CreERT2* mice were purchased from Shanghai Model Organisms Center, Inc. *Tie2Cre-Notch1*$^{fl/-}$ mice were obtained by crossing *Tie2Cre-apoE*$^{-/-}$ mice with *Notch1*$^{fl/-}$*apoE*$^{-/-}$ mice. *Hexb-CreERT2-DLL1/Jagged1*$^{fl/fl}$ mice were obtained by crossing *Hexb-CreERT2* mice with *DLL1*$^{fl/fl}$*Jagged1*$^{fl/fl}$ mice. All mice were bred on a C57BL/6 background and maintained under pathogen-free conditions. All mice of both sexes used in this study were housed with no more than five animals per cage under standardized light-dark cycle conditions with ad libitum access to food and water. The vivarium was maintained under controlled temperature (21 ± 1°C) and humidity (50–60%). The experimental procedures used in this study were approved by the Animal Care and Use Committees of Tianjin Medical University General Hospital (protocol approval number: 2022-DW-74).

Cell lines

THP-1 cells (ATCC, catalog TIB-202) were grown at 37°C, 5% CO_2 in 1640 medium with 10% fetal bovine serum.

Primary cells

Human umbilical vein endothelial cells (HUVECs) were isolated and cultured as described.[34] Briefly, the umbilical vein was perfused with Hank's balanced salt solution containing antibiotic/antimycotic (penicillin, streptomycin, and fungizone), and incubated at 4°C. After 1 h, the umbilical vein was drained, filled with collagenase, and incubated at 37°C for 15 minutes. The collagenase solution with cells was flushed from the vessel, cultured on plates coated with 50 μg/mL collagen. Cells were maintained in medium 199 (M199) supplemented with 20 mmol/L HEPES, pH 7.4, 10% FBS, 5 ng/mL of recombinant human fibroblast growth factor, antibiotics/antimycotics, and 90 μg/mL of heparin (EC medium). Mouse aortic endothelial cells (MAECs) were isolated and cultured as described.[35,36] After anesthesia, aortas were removed from WT male mice; the attached adipose tissue and connective tissue were excised and cleaned free. Aortas were cut into 1 mm rings, and opened longitudinally, and seeded, with lumen side down, onto collagen matrix–coated 12-well plates. The endothelial sprouting at day 2. The segments were removed and the cells were cultured continually until they reach confluence.

METHOD DETAILS

MCAO

After anesthesia, 8- to 12-week-old mice were subjected to intraluminal occlusion of the middle cerebral artery (MCA) was performed with a filament, as described.[37,38] A midline neck incision (4 mm–5 mm) were created, the common carotid artery and left external carotid artery were isolated and ligated. A rounded tip 6-0 nylon filament was introduced via a small incision in the common carotid artery and inserted into the internal carotid artery, to induce occlusion of the right MCA. After 60 min of occlusion, the occluding filament was withdrawn. Body temperature was monitored throughout surgery with a rectal probe and maintained at 37.0 ± 0.5°C using a heating pad. Sham-operated mice underwent the identical surgical procedures, but were not subjected to occlude the middle cerebral artery.

Drug administration

Mice were treated with anti-VCAM1 mAb (5 mg/kg/week, Sigma-Aldrich) or anti-Notch1 mAb (5 mg/kg/week, Biolegend) via intraperitoneal injection following MCAO or sham surgery. Mice received GW4869 (1.28 μg/g/2 days, MedChemExpress) via intracerebroventricular injection prior to MCAO and every 2 days thereafter until the end of experiment. Mouse IgG1κ (MedChemExpress) were used as the controls.

^{18}F-FDG PET imaging

At day 3 after MCAO, mice received an intravenous injection of 100 μCi ^{18}F-FDG at 1 h before scanning. Mice were then scanned by using a MicroPET small animal scanner (Bruker, Billerica, MA, USA), images were acquired on a field of view of 80cm x 80cm (160 x 160 pixel), and then reconstructed to a three-dimensional projection (336 x 160 x160 pixel). T2-weighted images of each animal were previously[39] acquired by a 7-T MRI scanner (Bruker) to delineate the regions of interest. PET and T2 images were fused to localize the vertebral bone marrow and data were calculated as mean standard uptake value (SUV). Mice were anesthetized by inhalation of 3.5% isoflurane and maintained by inhalation of 1.0% to 2.0% isoflurane in 70% N_2O and 30% O_2 during all scanning.

Intravital microscopy

Monocytes and neutrophils-endothelial interactions were analyzed by intravital epifluorescence microscopy as previously described.[40,41] At day 3 after MCAO, mice received anti-Gr1 mAb (Biolegend) to label monocytes and neutrophils and oregon green 488 dextran (MW: 70 kDa, 0.1 mL of 1% in saline) via tail vein injection. At 1 h later, mice were anesthetized and underwent laparotomy for exposing the mesenteric microvessels. Intravital microscopic imaging was performed using an Olympus FV1000 microscope and a 25x immersion objective.

Single-cell preparation

Mice were sacrificed by terminal anesthesia, after perfusion, the aorta was surgically removed, rinsed with ice-cold PBS, dissected into small pieces and incubated in digestion solution (60 U/mL DNase I (Sigma-Aldrich), 450 U/mL collagenase type I (Gibco), and 1 mg/mL BSA (Solarbio)) at 37°C water bath for 30 min, shaking the suspension every 10 min. Next, the cell suspension was filtered through a 70 μm cell strainer (Corning) and the cell strainer was rinsed with a FACS buffer (containing 2% BSA), 2 mM EDTA (Solarbio). The cell suspension was centrifuged at 300 g for 5 min. The cell suspension was enriched for ECs using CD31 MicroBeads (Miltenyi Biotec). CD31 enriched single cell suspension was stained with CD45- PerCP/Cy5.5 (Biolegend); CD31-APC (Biolegend). $CD45^{-}CD31^{+}$ ECs were sorted by FACS Aria III.

Single-cell RNA sequencing

Library Preparation and Sequencing

Single cell suspensions of isolated ECs were resuspended in PBS containing 0.04% ultra-pure BSA. scRNA-seq libraries were prepared using the Chromium Single Cell 3' Reagent Kits v2 (10x Genomics; Pleasanton, CA, USA) according to the manufacturer's instructions. The generated Single Cell 3' libraries were sequenced on an Illumina HiSeq4000, followed by de-multiplexing and mapping to the mouse genome (build mm10) using CellRanger (10x Genomics, version 2.1.1).

Data processing

Cell Ranger (http://support.10xgenomics.com/single cell/software/overview/welcome) uses the STAR aligner (https://github.com/alexdobin/STAR), which performs splicing-aware alignment of reads to the genome. The following quality control steps were performed: (1) genes expressed by less than 3 cells; (2) cells expressed less than 200 or more than 8000 genes and mitochondrial genes > 6%. Data was integrated, dimensionality reduction, clustered and visualized. Seurat was used for these processes. Cell counts were normalized and converted to the log scale with the Normalized Data and scaled with the Scale Data function. Principal component analysis (PCA) was performed and harmony v1 integration method was used to correct the potential batch effect. Top twenty principal components and ''resolution = 0.5'' were performed for clustering. EC clusters were annotated based on the expression of known endothelial cell and non- endothelial cell marker genes, including Pecam1, Cdh5 and Erg (endothelial cell), Acta2 and Tagln (smooth muscle cell), Dcn, Lum and Pdgfra (fibroblasts), Cd3d and Cd8a (lymphoid), S100a9, S100a8 and Cd14 (Myeloid) and Rgs5, Vtn (Pericyte). Contaminating cell clusters (non-ECs) were removed, and all downstream analysis was performed on ECs only.

The ''FindMarkers''(min.pct: 0.2; logFC threshold: 0.2; adjusted p value < 0.05) was applied to compare endothelial cell gene expression across conditions (sham and MCAO). The gProfiler (https://biit.cs.ut.ee/ gprofiler/gost) was used to measure over-representation of defined gene list against the Gene Ontology (GO) database (http://www.geneontology.org). Enriched biological processes of GO (BP, data version released in 2020) and the enrichment score ($-\log_{10}$ of the adjusted p value) for each pathway were reported.

Cellular senescence detection

A green florescence senescence detection kit (Invitrogen) was used to determine β-galactosidase expression. The staining process followed the vendor's manual. In brief, the mice were killed, and single-cell suspensions of aortas were collected. After staining with cell surface markers, cell suspensions were incubated with working solution at 37°C for 2 h without CO2. After washing in PBS, cells were analyzed with flow cytometry using IDEAS 6.2.

Flow cytometry

Mice were sacrificed by terminal anesthesia, after perfusion, aorta and brain were then collected for dissociation of cells. For aorta, single-cell suspensions were prepared as described above. The obtained single cells were co-labeled with CD45, CD31, VCAM1 and Notch1 in FACS buffer (30 min, 4°C); then to measure P16, P53 in endothelial cells, cells were permeabilized by using the BD Cytofix/Cytoperm Fixation/Permeabilization Kit, then incubated with p53 (DO-1) (Santa Cruz Biotechnology), p15 INK4B/p16 (Santa Cruz Biotechnology) at 4°C for 45min. Cells were then washed and suspended in FACS buffer. Whole brain was minced and incubated in digestion solution (60 U/mL DNase I (Sigma-Aldrich), 450 U/mL papain (Absin) at 37°C water bath for 30 min, myelin debris were removed by centrifuging in 30% percoll (Sigma Aldrich), cell pellet was then washed by PBS and resuspended in FACS buffer. The cell suspensions were stained with CD45, CD11b, DLL1 and Jagged1 at 4°C for 45min. Cells were then washed and suspended in FACS buffer. Data were collected by a FACSAria III flow cytometer and analyzed with FlowJo software.

To analysis source of plasma exosome, the exosome suspensions were stained with P2RY12, CX3CR1, CD171, GFAP, DLL1 and Jagged1 at 4°C for 45 min, then washed with PBS and pelleted by ultracentrifugation. Data were analyzed with flow cytometry using IDEAS 6.2.

Purification of plasma exosome

Exosomes from plasma were isolated using the Total exosome isolation kit (Invitrogen) as described.[42] In brief, plasma samples were centrifuged at 2,000 g for 20 min at room temperature. Thereafter, the supernatant containing the partially clarified plasma was transferred to a new tube without disturbing the pellet. The new tube was centrifuged at 10,000 g for 20 min at room temperature to remove debris. Then, the required volume of clarified plasma was transferred to a new tube. 0.5 volumes of PBS and 0.2 volume of the

Exosome Precipitation Reagent (from plasma) were added to the sample. After incubated at room temperature for 10 min, the samples were centrifuged at 10,000 g for 5 min at room temperature, and then the exosomes were resuspended in PBS.

Characterization of purified exosomes

For verification of purified exosomes using electron microscopy, exosomes suspended in PBS were dropped on formvar carbon-coated nickel grids and incubated for 10 min at room temperature. After staining with 2% uranyl acetate for 3 minutes at room temperature, micrographs were observed under a transmission electron microscope (Hitachi HT7700). The size and concentration of exosomes isolated from mice or patients' plasma were determined using a NanoSight NS300 (Malvern Instruments).

ELISA

Notch1 ligands and HMGB1 were measured by ELISA kits (FineTest EM6642, EM2010, EM2011, EM1918, EM7320, EH4500, EH0115 and EM0382) according to the manufacturer's instructions.

The exosome–EC binding assay

To verify the interactions between circulating exosomes and EC, exosomes were stained with CFSE in 100 μl PBS, and then washed with 10 ml PBS and pelleted by ultracentrifugation. ECs were treated with CFSE-labelled exosomes (15 μg/ml) for 2 h, then fixed for flow cytometry analysis.

To block exosomes binding to the Notch1 receptor of ECs, ECs were pretreated with anti-Notch1 antibodies (10 μg/ml) or IgG isotype antibodies (10 μg/ml) for 2 h, then incubated with ischemic stroke patients' plasma-derived exosomes (15 μg/ml) or exosome-depleted plasma for 24 h. For VCAM1 blocking *in vitro*, ECs were pretreated with 25 μg/ml Anti-VCAM1 mAb or IgG isotype antibodies (25 μg/ml) for 2 h, then incubated with ischemic stroke patients' plasma-derived exosomes (15 μg/ml) or exosome-depleted plasma for 24 h. The treated cells were then collected and analyzed by real-time PCR or flow cytometry.

Total-RNA isolation and real-time PCR analysis

Total RNA was extracted from cells with EasyPure RNA Kit (TransGen Biotech). RNA was reverse-transcribed to cDNA with SuperScript III and random primers (Thermo Fisher Scientific). TransStart Top Green qPCR SuperMix (TransGen Biotech) was used in real-time PCR and the ABI 7900HT Real-Time PCR System. The mRNA were quantified by 2-ΔCt [ΔCt = Ct (gene of interest) − Ct (β-actin)].

Cytokine array analysis

Plasma-derived exosomes from ischemic stroke patients and controls were collected for proteome profiling (Wayen Biotechnologies, Shanghai, China).

Cell adhesion assay

THP-1 cells were labeled with CellTrace calcein red-orange AM (Thermo Fisher Scientific) for 30min at 37°C, then plated onto HUVEC plates at 2×10^6 cells/well of 12-well plate. After incubation for 1h at 37°C, nonadherent cells were removed by washing 3 times with PBS, and the adhered platelets were fixed with HUVECs in paraformaldehyde solution 4% in PBS for 10 min. The numbers of stained adhering cells in 5 random fields were counted under a fluorescence microscope.

Atherosclerotic lesion analysis

Mice aorta tissues were fixed in 4% paraformaldehyde solution and stained with Oil-red O to quantify the lesion area. To analyze the lesion area in aortic roots, specimens were immersed in OCT and immediately frozen, then 7-μm sections were prepared and placed on glass slides. Serial cryosections from each mouse were stained with Oil-red O to evaluate lipid accumulation. Haematoxylin-eosin (HE) and Masson's trichrome staining was performed for morphometric lesion analysis. Images of plaques were captured under a Leica microscope, and quantitative analysis involved using Image-Pro Plus (Media Cybernetics, USA). For immunostaining, aorta sections were fixed with 4% paraformaldehyde for 10 min, washed with PBS, then blocked with normal goat serum for 30 minutes at room temperature, next incubated with primary antibody (anti-CD68 mAb: 1:100 or anti-αSMA mAb: 1:400) at 4°C overnight. After being washed 3 times in PBS, the sections were incubated with secondary antibodies for 1 h at room temperature, then mounted with flourished mounting medium with DAPI. Images were captured under a Zeiss confocal laser scanning microscopy.

Quantification of circulating lipid

Mice plasma was separated by centrifugation. Total plasma cholesterol (CHO), triglycerides (TG) and high-density lipoprotein cholesterol (HDL-C) and low-density lipoprotein cholesterol (LDL-C) were measured by using kits (BioSino Bio-Technology and Science).

Neuroimaging

Infarct volume was quantified on images acquired by a 7T MRI scanner (Bruker) as described.[37] T2-weighted images of the brain were acquired with fat-suppressed rapid acquisition with relaxation enhancement (RARE) sequence (repetition time, 4000 ms, echo time, 60 ms, slice thickness, 0.5 mm). Susceptibility-weighted images (SWI, repetition time, 21.0 ms; echo time, 8.0 ms; 0.3 mm thickness) were scanned. The MRI data were measured via image J (National Institutes of Health).

Histology assessment

The MCAO mice brains were fixed in 4% paraformaldehyde. Afterwards, brain tissues were fixed in optimum cutting temperature compound (O.C.T., Tissue-tek) solution and 10 μm coronal sections were cut on every 400 μm. Cresyl violet staining of coronal sections of infarcted brain was performed according to the manufacturer's protocol (Solarbio, G1430).

QUANTIFICATION AND STATISTICAL ANALYSIS

Power analysis and sample size calculations were performed using SAS 9.1 software (SAS Institute Inc.), and based on our experience with the respective tests, variability of the assays and inter-individual differences among experimental groups. The experimental design was based on our prior publications with similar mechanistic studies completed in our laboratory.[39,43,44] Animals were randomly assigned to experimental groups, based on the random number generator function in Microsoft Excel. All experiments presented in this study were repeated at least three times. A two-tailed unpaired Student's t test was used to compare data from two independent groups. One-way Analysis of variance (ANOVA) followed by Tukey post hoc test was used to compare data from three or more groups with one variable. For comparison of two or more variables among multiple groups, two-way ANOVA followed by Tukey post hoc test was used. $P < 0.05$ was considered to be significant. Data were analyzed with GraphPad prism 8.0. All data were presented as mean ± SEM.